CADMIUM PHOTO-IONIZATION LASER

by

REKHA TAMBAY

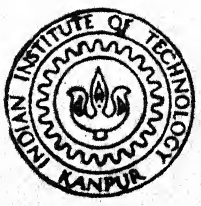

DEPARTMENT OF PHYSICS
INDIAN INSTITUTE OF TECHNOLOGY KANPUR

December, 1991

CADMIUM PHOTO-IONIZATION LASER

A Thesis Submitted
In Partial Fulfilment of the Requirements
for the Degree of

DOCTOR OF PHILOSOPHY

by

REKHA TAMBAY

to the

DEPARTMENT OF PHYSICS
INDIAN INSTITUTE OF TECHNOLOGY KANPUR

December, 1991

PHY-1991-D-TAM-CAD

CERTIFICATE

Certified that the work contained in the thesis entitled "CADMIUM PHOTO-IONIZATION LASER" has been carried out by Ms. Rekha Tambay under my supervision and the same has not been submitted elsewhere for a degree.

Kanpur
December , 1991

(R K THAREJA)
Thesis Supervisor
Department of Physics
I.I.T. Kanpur

SYNOPSIS

Name of student : REKHA TAMBAY Roll # : 8520964
Degree for which submitted: Ph.D. Department: Physics

Thesis Title : CADMIUM PHOTO-IONIZATION LASER

Name of thesis supervisor : Dr R.K. Thareja

In this thesis we studied cadmium metal vapor plasma in a crossed heat pipe. Laser oscillations in Cd II on $4d^9\ 5s^2\ ^2D_{5/2} - 4d^{10}5p\ ^2P_{3/2}$ transition at 441.6 nm were observed using photo-ionization pumping through soft x-rays from a laser produced tungsten plasma. Mach Zehnder Interferometer was designed for measurement of electron density of the plasma. Studies on laser produced Al plasma were also performed to see the dependence of electron temperature on intensity and wavelength of laser radiation. For plasma production we used a Nd:YAG laser and its harmonics $2\omega_o$, $3\omega_o$, $4\omega_o$. While optimizing the parameters of the laser, studies on laser induced air breakdown were performed in a vacuum chamber and in laboratory air. The dependence of pulse width and pressure was studied using Nd:YAG laser and its harmonics. The breakdown threshold

scales as $p^{-0.8}$ for 1.06 μm, while a weak scaling of $p^{-0.4}$ was observed for 0.532 and 0.355 μm wavelength. We observed that the threshold field scales with laser pulse t_p as $t_p^{-0.5}$ for 0.532, 0.355 and 0.266 μm. For 1.06 μm a scaling of $t_p^{-0.35}$ is observed.

To study metal vapor plasma and laser oscillations a crossed heat pipe of 1" dia stainless steel tube was designed. A stainless steel mesh was inserted in all the four arms. The arm length was 16 cm. Water cooling arrangement was provided to cool the four ends of the heat pipe. Cadmium metal was kept at the center of the heat pipe. The center of the heat pipe was heated using a heating tape. The central zone of the heat pipe was covered with a brick structure to reduce convection losses. Helium was used as a buffer gas. At higher temperatures (>500°C) cluster formation of cadmium was observed. To check it, a low power HeNe laser beam was sent close to the center of the heat pipe. The convective movement of dust like particles was observed in the transmitted beam. The optimum temperature of the heat pipe at which no clusters were formed was 420°C in our system.

Studies on laser produced Al plasma were perfomred in a target chamber evacuated to 10^{-3} Torr. A Nd:YAG laser and its

harmonics were used for plasma production. Electron temperature was estimated by assuming the plasma to be in local thermodynamic equilibrium. The temperature was estimated to be in the range 0.8 _ 4.0 eV. The electron density ~$2x10^{16}$ cm^{-3} was estimated by measuring the stark width of Al II line on $4p\ ^1P_1 - 4d\ ^1D_2$ transition at 559.3 nm . Variation of electron temperature with intensity of laser radiation gives $I^{0.3}$ dependence. The temporal profile of Al I, Al II and Al III are recorded to estimate the velocity of the plasma front.

Studies on cadmium metal vapor plasma were performed in the heat pipe. To start with system was baked for several hours. Once it is ready cadmium metal was kept at its center. After evacuating the heat pipe to a pressure of $\leq 10^{-4}$ Torr, helium was filled in at required pressure, and the temperature was set to the desired value. Cadmium vapor plasma was also studied in the presence of a background plasma, tungsten in our case. The plasma was produced by focussing a Nd:YAG laser on to the tungsten target for tungsten plasma or at the center of the heat pipe while looking for pure metal vapor plasma. The plasma emission was imaged on to the monochromator slit. The output from the monochromator was detected with a photomultiplier tube (PMT). The PMT output was recorded on a strip

chart recorder. We observe an increase in intensities of all the lines of cadmium in the presence of tungsten plasma. The electron temperature was estimated to be 0.5 eV for pure metal vapor plasma by assuming the plasma to be in local thermodynamic equilibrium (LTE). The plasma density was estimated by using a Mach Zehnder Interferometer where the heat pipe formed one arm of the Interferometer. A compensating glass plate was inserted in the reference arm. A well collimated beam of second harmonic (0.532 μm) of Nd:YAG laser was used as a probe beam. By measuring the shift in the fringes because of change in refractive index electron density of the plasma can be estimated. The interferograms were recorded, enlarged digitized and analysed using Abel inversion. The electron density of tungsten plasma at 2 mm from the tungsten target surface is estimated to be $6 \times 10^{18} cm^{-3}$.

The cadmium photo-ionization laser on $4d^9\ 5s^2\ {}^2D_{5/2}$ - $4d^{10}\ 5p\ {}^2P_{3/2}$ transition at 441.6 nm was observed in a heat pipe. The heat pipe was operated at 420°C and helium at a pressure of 7 Torr was used as a buffer gas. Using a temperature controller it was ensured that temperature of the heat pipe remains within ±5°C. During this temperature variation the vapor pressure of the cadmium remains nearly

constant. The soft x-rays (blackbody) emitted from a tungsten plasma was used as a pumping source for cadmium vapors. Two He-Cd mirrors of 2m radius of curvature forms the cavity. One of the mirrors is totally reflecting while the other has about 1% transmission at 441.6 nm, through which the laser output was monitored. The output was detected through a monochromator using a photomultiplier tube. The signal was seen on a storage oscilloscope. The output signal is sensitive to the alignment of the resonator axis with a slight movement of either mirror the stimulated emission falls to a very low level. The optimum value of the resonator axis is found to be 4 mm away and parallel to the target surface. To see the effect of the input laser energy (Nd:YAG) on the output of Cd II laser at 441.6 nm, experiment was performed at 100, 200, 300 mJ of input energy in 8.0 nsec (FWHM) pulse. We observe that the Cd II laser output increases with the input laser energy. The electron density of the plasma was estimated by recording the interferograms at different distances from the target surface using a Mach Zehnder Interferometer. We estimate the electron density of cadmium plasma in the presence of tungsten plasma at 4 mm from the tungsten target to be 1.4×10^{19} cm^{-3}.

ACKNOWLEDGEMENTS

I am deeply indebted to Dr. R.K. Thareja for introducing me to the subject. Without his full support and cooperation, it would have not possible for me to complete this work. I gained a lot from his suggestions during the course of work.

Initial motivation and encouragement have got from my seniors, Alika and Vinay. I express my sincere thanks to them.

I want to express my sincere thanks to all my lab mates Rangit, Prasad, Abhilasha and Anup, for helping me in finalising the thesis.

I would like to thank all the staff members of CELT & Physics office and Workshop, Glass Blowing lab for providing timely help.

I must thank to Mr. G.R. Hoshing for typing the manuscript and Mr. Jain for preparing the tracings.

Finally, wish to express my deep sense of gratitude to my family members, specially to my mother and my husband for their encouragement and support.

Rekha Tambay

Dedicated

To

My Late Father

LIST OF PUBLICATIONS

1. Rekha Tambay, D. victor Suvisesha Muthu, V. Kumar and R.K. Thareja, "Laser Induced Air Breakdown using 0.355, 0.532 and 1.06 μm Radiation", Pramana, J. Phys. 37, 163 (1991).
2. Rekha Tambay and R.K. Thareja, "Laser Induced Breakdown Studies of Laboratory Air at 0.266, 0.355, 0.532 and 1.06 μm", J. Appl. Phys. 70, 2890 (1991).
3. Rekha Tambay and R.K. Thareja, "Studies of Metal Vapor Plasma in the presence of a High Z Target Laser Produced Plasma", J. Appl. Phys. (Submitted).
4. Rekha Tambay, Ranjit Singh, and R.K. Thareja, "Studies on Recombining Al plasma using 1.06, 0.532, 0.355, 0.266 μm Laser Radiation", J. Appl. Phys. (Submitted).
5. Rekha Tambay and R.K. Thareja, "Cadmium Photo-ionization Laser", Opt. Lett. (Submitted).

TABLE OF CONTENTS

LIST OF FIGURES

LIST OF SYMBOLS

P_{pi}	Photo-ionization pumping rate
c	Velocity of light
N_{ν}	Photon density
Ω	Solid angle
W_p	Pumping power
$h\nu_p$	Energy of the pumping photon
σ_t	Total absorption cross section
N	Ground state population density of metal vapors
k_f	Conversion efficiency of the incident flux into soft x-ray flux
T	Temperature in $^{\circ}C$
T_e	Electron temperature
I	Intensity of the laser radiation
τ	Laser pulse width
λ	Wavelength
$\Delta\phi$	Phase shift
λ_p	Probe wavelength
μ	Refractive index of the plasma
ω_p	Plasma frequency

n_e	Electron density
ν_e	Electron collision frequency
m	Electron mass
e	Electron charge
ϵ_o	Permittivity of free space
r_o	Size of the plasma
Δ	Fringe spacing
a_{ij}	Abel coefficient
f	Lens focal length
P	Pressure
E	Excitation energy
g	Statistical weight
W	Electron impact parameter
g_c	Gaunt factor
k_B	Boltzman constant

CHAPTER I

INTRODUCTION

The first proposal for observing population inversion in VUV and x-ray region was suggested by Duguay and Rentzepis[1] in 1967. They suggested of removing an inner shell electron from sodium atom leaving the ion in an excited state, which was inverted with respect to the ion ground state resulting in laser oscillation on $3s^1P_1$-$2p^1S_o$ transition at 37.2 nm. The x-ray filters were used to eliminate unwanted spectral components from the pumping source. The large separation between the pumping source and the active medium resulted in loss of the pumping flux. Harris et al[2] suggested using a laser produced plasma source within the vapor or gas to be excited for reducing the separation between the source and the excitation region. Using this configuration they observed Li^+ ion density ($4x10^{15}cm^{-3}$) in a heat pipe oven using laser produced tantalum plasma. Silfvast et al[3] were the first to demonstrate photo-ionization laser using soft x-rays from the laser produced tantalum plasma as a pumping source. Since then there have been many reports[4,5] on the observation of population inversion using x-ray pumping. A variant of the

scheme using multispot plasma has been reported by Hube et al[6]. They also reported[7] photo-ionization laser in cesium vapor in the range 665-800 nm. Lundberg et al[8] observed inversion densities in Zn^+ at 747.8 nm by photoionizing inner d shell electron with a broad band soft x-ray source. Similar arrangement has been used to study Auger pumped lasers in xenon (108.9 nm) and krypton (90.7 nm) by Kapteyn et al[9]. The lasers are pumped by photo-ionization of inner shell electrons followed by Auger decay into excited states. Recently a magnesium photo-ionization laser at 24.7 nm has been proposed[10].

Various excitation techniques used to get population inversion in short wavelength regime are;

1. Electron collisional excitation pumping
2. Electron collisional recombination pumping
3. Charge transfer pumping
4. Photo-excitation pumping
5. Photo-ionization pumping.

1. Electron Collisional Excitation Pumping :

The electron collisional excitation technique is usually used with ion lasers in the near UV region. The pumping process is described by the equation,

$$X_o^{i+} + e \rightarrow X_u^{i+}$$

It is inherently CW in nature in the sense that, final level is the ground state itself, and that only one ionic species is involved in this process. Ions with ground state configuration $1s^2\ 2s^2\ 2p^n$, neon like sequence have been proven to be most successful. Lasing in Ne like, Ge^{22+} and Cu^{19+}, in the wavelength interval of 19.5-28.5 nm was observed by Lee et al[11]. The scheme has also been used for Ni like ions. Soft x-ray amplification in Ni like, Eu^{35+} at 6.58 and 7.1 nm has been reported by MacGowan et al[12]. Gain measurements for soft x-ray laser in Ni like, W^{46+} have been carried out by Maxon et al[13].

2. Electron Collisional Recombination Pumping :

This scheme has been successful mostly on hydrogen like and Li like sequences. In this scheme ions are created in some charge state Z. Input energy may be supplied from an electric discharge, an arc or a laser beam. Large amount of energy required to disturb the thermal equilibrium of level populations result in highly ionized plasma. Electrons are cooled by allowing it to expand, or by collisions with some background gas and recombine with ions, to go to some highly excited levels of the next lower charge state (Z-1). These bound electrons move downwards via collisions until they reach a significant gap in the energy level where the collisional decay rate is significantly reduced. The population starts building up just above this gap. An inversion would occur with respect to one or more lower levels resulting in laser action across the gap. The first recombination laser was observed by Latush et al[14] in Ca and Sr. Population inversion in Carbon[15], Potassium[16], Helium[17], Aluminium[18] have been observed using recombination pumping. Gain measurement studies at 18.2 nm in carbon have been performed by Kim et al[19]. Silfvast et al[20] proposed segmented plasma excitation and recombination (SPER)

technique to observe laser oscillations in recombining electrical discharge plasma. Studies on cadmium plasma recombination laser have been reported by Khare and Thareja[21]. Recombination pumped laser action on carbon VI Balmer α line (18.2 nm) has been described by Daido et al[22] in a wall confined plasma. Soft x-ray amplification of lithium like aluminium in recombining plasma have been studied by Jaegle et al[23]. Laser amplification at 18.2 nm in recombining plasma from a laser irradiated carbon fiber has been observed by Popovics et al[24].

3. Charge Transfer Pumping :

In this scheme the ion acquires an electron in an upper laser state from a neutral atom, rather than from an electron. The dominant single electron exchange process can be described by,

$$X_o^{(i+1)+} + Y \rightarrow Y^+ + X_u^{i+}$$

for a neutral perturbing atom Y impacting on a (i+1) times ionized target ion X. The process is energy-resonant between the binding energies of the electron in the ground state of the atom and that of the upper laser state of the target ion.

Resonance charge transfer and population inversion following C^{5+} and C^{6+} interaction with carbon atoms in a laser produced plasma have been reported[25].

4. Photo-excitation Pumping :

This pumping scheme requires precise matching of the pump and the absorbing transition energies. The process can be described by the equation,

$$X_o^{i+} + h\nu \longrightarrow X_u^{i+}$$

Selected upper state is populated from the ground state by absorption of photons at the proper frequency, so it avoids the problem of a larger pumping rate for the lower laser state and therefore, the need for a metastable upper state. The pumping rate required in photo-excitation pumping is less than the rate required in electron collisional excitation pumping. Another advantage of photo-excitation pumping is that, the pumping and the specific upper laser level can be controlled by the photon flux and chosen wavelength respectively. In this scheme one dense plasma provides the photons in a spectral line and another adjacent plasma with an appropriate absorption line in an ion serves as the laser medium. Lasing in Al XII at 4.4 nm

pumped by Si XIII have been observed by Apruzese et al[26]. Experiments performed[27] using composite targets of carbon and magnesium indicate population inversion in Mg^{10+} and Mg^{11+} at 10 nm. Fluorescence and gain measurements at 217.7, 216.3 nm in C III by photo-excitation with Mn line radiation at 31 nm have been reported[28-30]. Recently Apruzese et al reported[31] gain in Al XI pumped Mg IX, at 22.8 nm.

5. Photo-ionization Pumping :

We have used photo-ionization pumping for observing laser oscillations in cadmium vapor at 441.6 nm using soft x-rays from laser produced plasma as a pumping source. When photons in the proper energy range impinge on an atom or ion there is a possibility that they will knock out an electron from the inner shell of the system. The energy of the incident photon is given to the electron, partly as its kinetic energy and partly as its binding energy. Such a creation of an inner shell hole can lead to a population inversion with respect to an outer shell or valence electron. In the photo-ionization pumping the final state lies in the continuum, although there are also resonances at various energies where bound discrete states

overlap and often interact with the continuum states. The process of photo-ionization can be described as,

$$X_o^{i+} + h\nu \longrightarrow X_u^{(i+1)+} + e$$

The rate of pumping for photo-ionization process is given by

$$P_{pi} = N_\nu \sigma_{pi} c \quad sec^{-1} \qquad (1)$$

where N_ν is the photon density of the pumping source and σ_{pi} is the photo-ionization cross section.

For most atoms the photo-ionization cross section lies between 10^{-19} - 10^{-17} cm^2. The cross sections for removing the outermost free electron rises at the ionization threshold and then falls with higher photon energy. At higher photon energies it is possible to remove electron from the inner shell. The photo-ionization cross section curve for sodium for removing electron from 3s, 2p and 2s states is shown in Fig.1. The curve shows that the cross section for removing 2p electron is more than one hundred times of that for ejecting the outer 3s electron. Thus it is possible to get population inversion in Na, on 3s $^1P_1$ - 2p ^1S_o transition, at 37.2 nm. Similarly the photo-ionization cross section curve for Cd, shown in Fig. 2

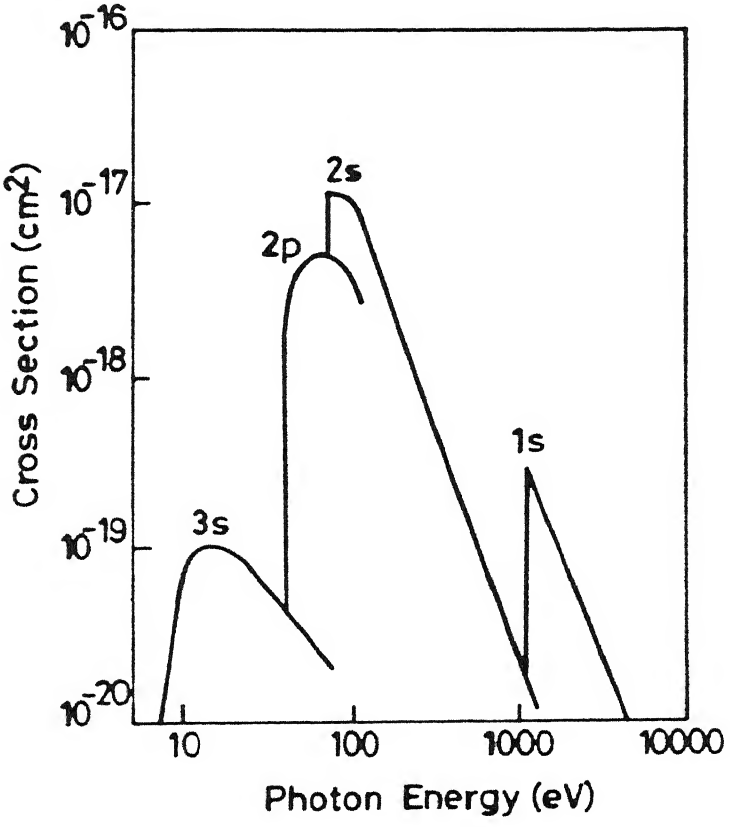

Fig. 1 Photo-ionization cross section of sodium.

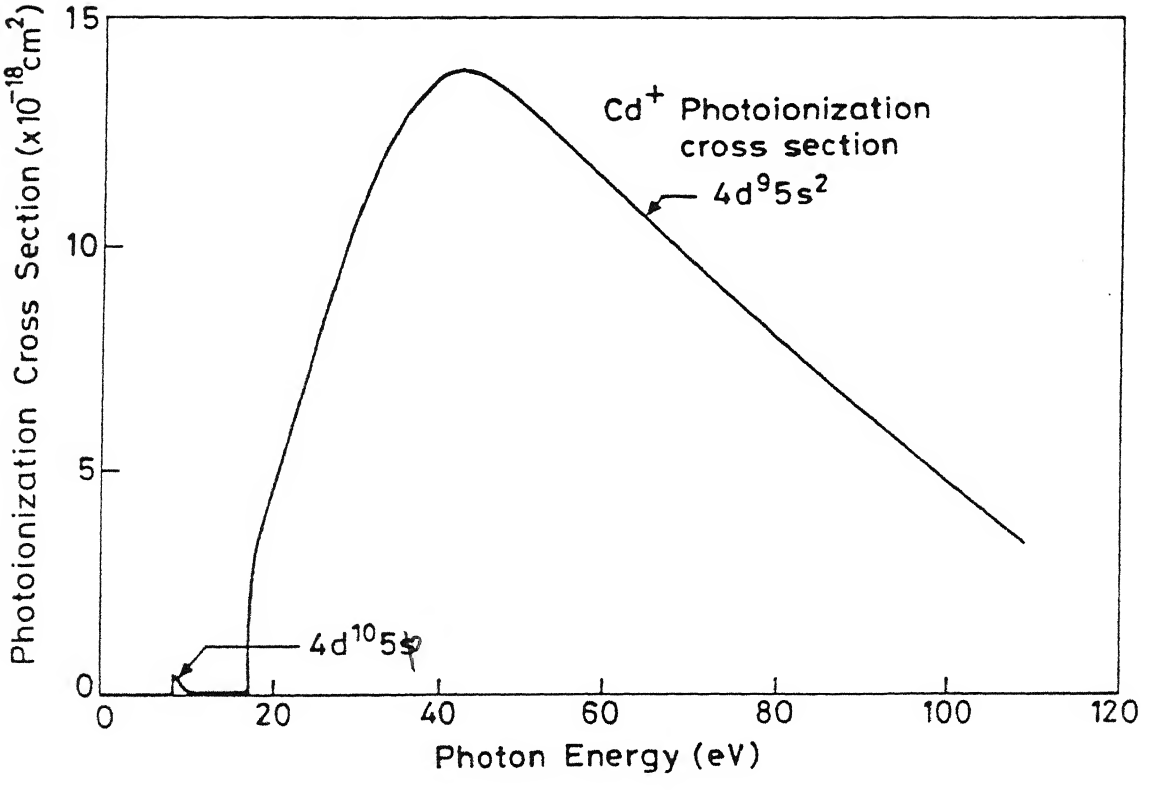

Fig. 2 Photo-ionization cross section of cadmium.

shows that the cross section for removing the inner shell 4d electron is large compared to the cross section for removing the $5s^2$ electron. Thus photo-ionization pumping can be used in cadmium also to get population inversion. Photo-ionization of atoms with nearly closed or closed outer shell arrangements leads to a minimum number of final states, and hence pumping efficiency is highest for such configurations. In cadmium the outer most s shell is closed and when inner d shell electron is photoionized, it leads to a final state which is split in just two levels, thus increasing the pumping efficiency.

Pumping Sources

Laser Produced Plasmas :

By focusing a high power laser on to a solid target, high temperature and high density plasma is formed close to the target surface. Besides laser energy and wavelength the plasma characteristics also depend on the physical properties of the target material. For lower irradiation, ($\simeq 10^6$ W/cm^2) the absorbed radiation appears as heat which is slowly distributed throughout the material by thermal diffusion. If the intensity is more than 10^6 W/cm^2, intense local heating can result in rise in surface temperature of the material. A further

increase in irradiation results in evaporation of the melted metal. Once the vapor is formed, further heating is caused by multiphoton ionization and inverse bremmstrahlung. The emission comprised of line as well as continuum radiation. For a high Z solid target, the continuum emission dominates[32] over line radiation and can be approximated as a blackbody in a thin layer close to the target surface with temperature of approximately the same as that of the plasma. For lower intensities ($\sim 10^{10}$ W/cm^2) the temperature[33] of the plasma is given by,

$$T \approx (I\lambda^2)^{4/9}$$

while for higher intensities ($\sim 10^{13}$ W/cm^2) the temperature scales as,

$$T \approx 0.6(I\lambda^2)^{2/3}$$

Studies[34] on laser produced plasmas from different target materials, in the intensity range 10^{11}-10^{12} W/cm^2 have shown that for high Z elements the peak of the emission spectrum is shifted towards shorter wavelength. Thus by choosing the target material we can match the emission spectrum with that of the photo-ionization cross section. The conversion efficiency of

laser energy into photon-flux in the soft x-ray region upto 50% has been reported[35]. Thus the soft x-rays emitted from laser produced plasmas of a high atomic number transition element such as tungsten, tantalum etc.[4-7], can be used effectively as blackbody sources. We used laser produced tungsten plasma as a pumping source for observing laser oscillations in Cd II on $4d^9\ 5s^2\ ^2D_{5/2}$ — $4d^{10}\ 5p\ ^2P_{3/2}$ transition at 441.6 nm.

Diagnostics of laser produced plasmas :

Pumping rate depends upon the photon density N_ν [eq. (1)]; N_ν effects density and temperature of a plasma, cadmium in our case. Thus it is necessary to estimate density and temperature of a plasma. The electron density of a plasma is usually measured employing the following techniques :

1. Optical diagnostic techniques
2. Spectroscopic techniques

The electron temperature of a plasma can be estimated by

1. Line intensity measurements
2. Langmuir probes

Density Measurements :

Optical Interferometry

Optical diagnostic techniques for plasma are used for measuring the refractivity of a plasma by directly comparing the phase of a wavelength passing through the plasma with a reference. The measurement of phase shift provide us the density of electrons[36].

The usually employed interferometers are

1. Michelson Interferometer
2. Fabry Perot Interferometer
3. Mach Zehnder Interferometer

We have used Mach Zehnder Interferometer[37] in our studies.

It is a two beam interferometer but differs from that of the Michelson interferometer in having two arms in which the beams travel in only one direction. A typical Mach Zehnder Interferometer is shown in Fig. 3. The interferometer consists of two beam splitters and two mirrors. The dispersive element, plasma in a heat pipe oven in our case, is kept in one arm of the interferometer and a compensating glass plate is inserted

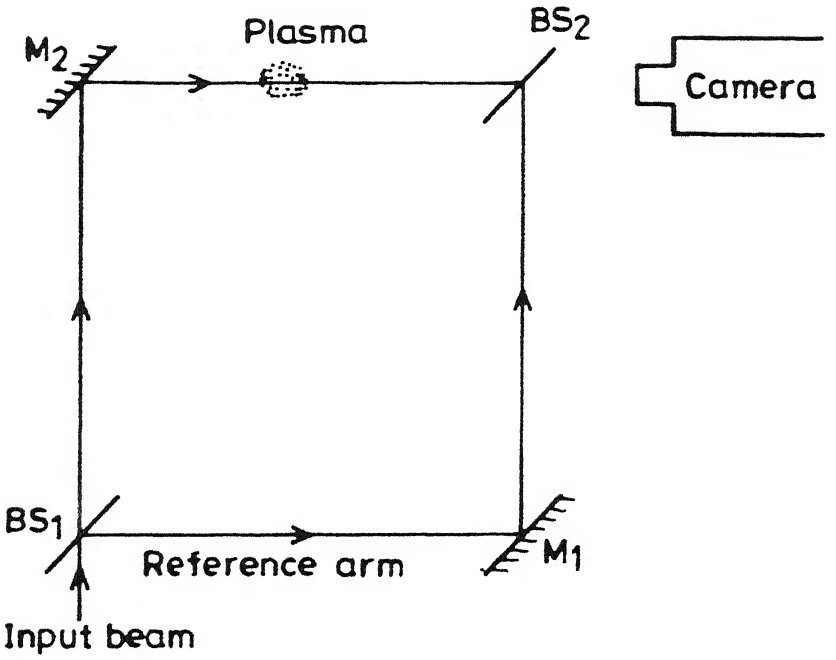

Fig. 3 Typical Mach Zehnder Interferometer.

in the reference arm to compensate the path difference between the two interfering beam. The phase difference between the two beams is given by,

$$\Delta\varphi = \frac{2\pi}{\lambda_p} \int_o^{r_o} (1-\mu)\, dy \qquad (2)$$

where μ is the refractive index of the plasma, and is given[33] as,

$$\mu = \left[1 - \frac{\omega_p^2}{\omega^2 + \nu_e^2} \right]^{1/2} \qquad (3)$$

ω_p is the plasma frequency given as $\omega_p^2 = \frac{n_e e^2}{m \epsilon_o}$ and ν_e is electron collision frequency[33] λ_p the probe wavelength, and r_o is the size of the plasma. Using eq. (3) in eq. (2) we have,

$$\Delta\varphi = \frac{2\pi}{\lambda_p} \int_o^{r_o} \left[1 - \left\{ 1 - \frac{\omega_p^2}{(\omega^2 + \nu_e^2)} \right\}^{1/2} \right] dy \qquad (4)$$

for $\omega^2 + \nu_e^2 > \omega_p^2$,

$$\Delta\varphi = \frac{2\pi}{\lambda_p} \int_0^{r_o} \frac{\omega_P^2}{2(\omega^2 + \nu_e^2)}\, dy \qquad (5)$$

when $\omega^2 >> \nu_e^2$ collisional effects can be neglected and eq. (5) reduces to

$$\Delta\varphi = \frac{e^2\lambda_p}{4\pi\epsilon_o mc^2} \int_0^{r_o} n_e\, dy \qquad (6)$$

It follows from eq. (6) that by measuring the phase shift, electron density n_e can be estimated.

Studies on measurement of densities of electron and neutral atoms in a carbon plasma have been performed by Charles David[38] using a two wavelength interferometry. Mach Zehnder Interferometer has been used for measuring densities of various atomic and ionic levels in the laser excited barium vapor[39]. The laser pulse that excited the Ba vapor was a 1 μs long dye laser pulse tuned at wavelength of 553.5 nm. The probe beam used for interferometric studies was a 1 nsec long broad band (417-608 nm) dye laser. Interferometric studies of laser induced surface heating and deformation of metal and semiconductor have been carried out by Lee et al[40]. Time

resolved electron density measurements in an ArF excimer laser discharge have been reported by Mochizuki et al[36] using He-N_2 laser (337.1 nm) as a probe beam. Recently density measurement of Ti atoms, in laser produced Ti vapor plasma has been reported[41]. The plasma was produced using a YAG laser of 1.5 ms duration, and a N_2 laser (337.1 nm) of 10 nsec pulse duration was used as a probe beam.

We have reported[42] measurement of density of tungsten and cadmium plasma in a heat pipe using Mach Zehnder Interferometer.

In addition to optical interferometry, Schliren[43] and Shadowgraphy[44] techniques have also been employed for density measurement. These techniques depend on deviation of the beam which is proportional to the first and second derivative of the electron density. In these techniques no separate reference beam is used; rather the intensity variations arise by virtue of local intensification of the probe beam due to refraction. Such systems are easy to align compared to interferometers but the analysis of the results is difficult.

Spectroscopic Techniques

The usually employed spectroscopic techniques are :

1. Resonance absorption
2. Using Stark broadening of a transition

We have used Stark broadened transition in Al II for estimating the density of the plasma.

Stark Broadening

Stark broadening of a transition can provide us the electron density. The Stark broadening is also known as pressure broadening or collisional broadening. It arises due to the perturbation of the energy levels of an atom or ion by changing electric fields occuring in a collision with a charged particle. When the ion and electron temperatures are of the same order than the Stark broadening caused by electron collisions is much higher than that caused by ions of the plasma. For a Lorenztian profile the Stark width is related to the electron density by eq.(16). Wiese et al[45] measured the Stark width of oxygen lines in an arc plasma to determine the electron density. Stark broadened profiles of C V and C VI

have been measured[46] to determine the electron density of laser produced plasma of polyethylene foil. Recently electron density measurement of plasma jets generated by a high pressure discharge capillary has been carried out by Aschkenazy et al[47], using the Stark broadening of the hydrogen H_α and H_β spectral lines.

Temperature Measurements :

Line Intensity Measurement

For a plasma in local thermodynamic equilibrium[48] the intensity ratio of spectral lines can provide us the electron temperature, if the population of various levels is related by Boltzmann distribution[48]. Electron temperature in an electric discharge produced Cd plasma have been measured[49] by taking intensity ratio of spectral lines. We have measured electron temperature of Cd plasma[42] and of laser produced Al plasma[50] using the intensity ratio of spectral lines.

Present Work

In the present work, we have studied cadmium vapor plasma in a heat pipe. Laser oscillations in Cd II on $4d^9\ 5s^2\ ^2D_{5/2} - 4d^{10}\ 5p\ ^2P_{3/2}$ transition at 441.6 nm were observed using

photo-ionization pumping through soft x-rays from a laser produced tungsten plasma. Mach Zehnder Interferometer was designed for measurement of electron density of the plasma. Studies on laser produced Al plasma were also performed. For plasma production we have used a Nd:YAG laser (DCR-4 Spectra Physics) and its harmonics $2\omega_o$, $3\omega_o$, $4\omega_o$ delivering upto 1J of energy in 8.0 nsec (FWHM) and 2.5 nsec (FWHM) at fundamental with a repetition rate of 10 pps. The laser was also used to study laser induced air breakdown.

The details of experimental techniques used for the present work are described in Chapter II.

Chapter III gives the details of the studies on laser produced Al plasma. The experiment was performed in a target chamber evacuated to 10^{-3} Torr. A Nd:YAG laser and its harmonics at $2\omega_o$, $3\omega_o$, $4\omega_o$ were used for plasma production. Electron temperature was estimated by assuming the plasma to be in local thermodynamic equilibrium. The temperature was estimated to be in the range $0.8 \leq T \leq 4.0$ eV. The electron density $\sim 2 \times 10^{16}/cm^3$ is estimated by measuring the Stark width of Al II line on $4p\ ^1P_1 - 4d\ ^1D_2$ transition at 559.3 nm. Variation of electron temperature with intensity of laser

radiation and wavelength was also studied. The temperature scales with intensity as $I^{0.3}$. The temporal profiles of Al I, Al II and Al III were measured to estimate the velocity of the plasma front.

Chapter IV describes the studies on cadmium metal vapor plasma in a heat pipe. We observed the formation of cadmium clusters in the overheated zones of the heat pipe. Cd vapor plasma was also studied in the presence of a background plasma, tungsten in our case. The plasma was produced by focussing a Nd:YAG laser on to the tungsten target for tungsten plasma or at the center of the heat pipe while looking for pure metal vapor plasma. We estimate the electron temperature 0.5 eV of pure metal vapor plasma by assuming the plasma to be in LTE[48]. The plasma density was estimated using a Mach Zehnder Interferometer[37] where the heat pipe forms one arm of the interferometer. The second harmonic (0.532 μm) of the Nd:YAG laser was used as a probe beam. The interferograms were enlarged, digitized and analyzed using Abel inversion[51,52]. The electron density at 2 mm from the target surface is estimated to be $6 \times 10^{18}/cm^3$.

The cadmium photo-ionization laser on $4d^9\ 5s^2\ {}^2D_{5/2}$ - $4d^{10}\ 5p\ {}^2P_{3/2}$ transition at 441.6 nm observed in a heat pipe is described in Chapter V. The soft x-rays (black body) emitted from a tungsten plasma was used as a pumping source. The laser output at 441.6 nm was found to increase with the input energy. To estimate the electron density, interferograms were recorded at different distances from the target surface using Mach Zehnder Interferometer. The probe beam used was the second harmonic (0.532 μm) of the Nd:YAG laser. The probe beam was delayed by 19 nsec with respect to the reference beam. We estimate the electron density of cadmium plasma at 4 mm from the tungsten target to be 1.4×10^{19} cm^{-3}.

Chapter VI summarises the results of the present work.

CHAPTER II

EXPERIMENTAL TECHNIQUES

Various experimental schemes for generating short wavelength lasers are described in Chapter I. We have observed laser oscillations in cadmium vapor on $4d^9\ 5s^2\ ^2D_{5/2} - 4d^{10}\ 5p\ ^2P_{3/2}$ transition at 441.6 nm using a blackbody pumping source from high Z plasma. The plasma density was measured using Mach Zehnder Interferometer[37]. Laser produced Al plasma was studied in a target chamber using all the four wavelengths of Nd:YAG laser and its harmonics $2\omega_o$ (0.532 μm), $3\omega_o$ (0.355 μm), $4\omega_o$ (0.266 μm). The electron density was measured using Stark broadened transition $4p\ ^1P_1 - 4d\ ^1D_2$ at 559.3 nm of Al II.

The homogeneous metallic vapors in the past were obtained using furnaces of different types; hot cathode diode, atomic beam devices, burner system or other similar instruments. However to get homogeneous temperature and density distribution, sophisticated radiation shields and heat baffles are to be used with most of these devices[53,54]. Another difficulty is that of the windows. Since at high temperature many vaporized species are highly reactive, vapors are kept away from windows by means of traps. Even for non reactive

vapors, the temperature of the windows is kept higher in order to prevent vapor condensation on the windows. Either of the techniques introduces uncertainties in determining the number density of particles because of poorly defined boundary layers. This uncertainty can be reduced by using a 'heat pipe' initially developed by Grover et al[55]. The heat pipe consists of a closed tube whose inner surface is lined with a porous wick. The wick is saturated with the liquid phase of the working fluid and the remaining volume of the tube contains the vapor phase. Heat applied by an external source vaporizes the liquid in the central section and a heat sink provided at the other end drives the liquid back by capillary forces to the central zone. Thus heat conductivity is achieved which is much larger than ordinary thermal conductivity.

The heat pipe offers many advantages over the previously used devices. They are a) the inert gas between the windows and the vapor zone removes problem of deposition on the windows specially for reactive species e.g., barium, lithium etc. b) The metal vapor is very clean because of the continuous evaporation and condensation of the metal. c) It can be operated continuously under extremely well known conditions of

temperature and pressure. The device has been successfully used in resonance fluorescence measurements of alkali molecules[56], harmonic generation in metal vapor gas mixture[57] and also for metal vapor lasers. In order to operate this device for spectroscopic and other measurements, the heat pipe is first filled with an inert gas at a suitable pressure with test metal at the centre of the heat pipe. The central portion is heated and the melted metal wets the wick. The metal vapor then diffuses towards both ends until it condenses again. The condensate returns to the evaporator section through wick. In steady state operation of a heat pipe there are three well defined regions as shown in Fig. 4. The ends A and A′ contain only the buffer gas. The central portion B is pure metal vapor zone. The boundary C and C′ consists of a mixture of buffer gas and metal vapor. Since the dynamics in heat pipe oven cannot be worked out in a simple way these conditions have been determined in an empirical way. It has been observed that if the central part of the heat pipe is overheated the conditions are changed[42,58].

The cross heat pipe used in our studies is shown in Fig. 4 (inset). The crossed heat pipe was made up of stainless steel

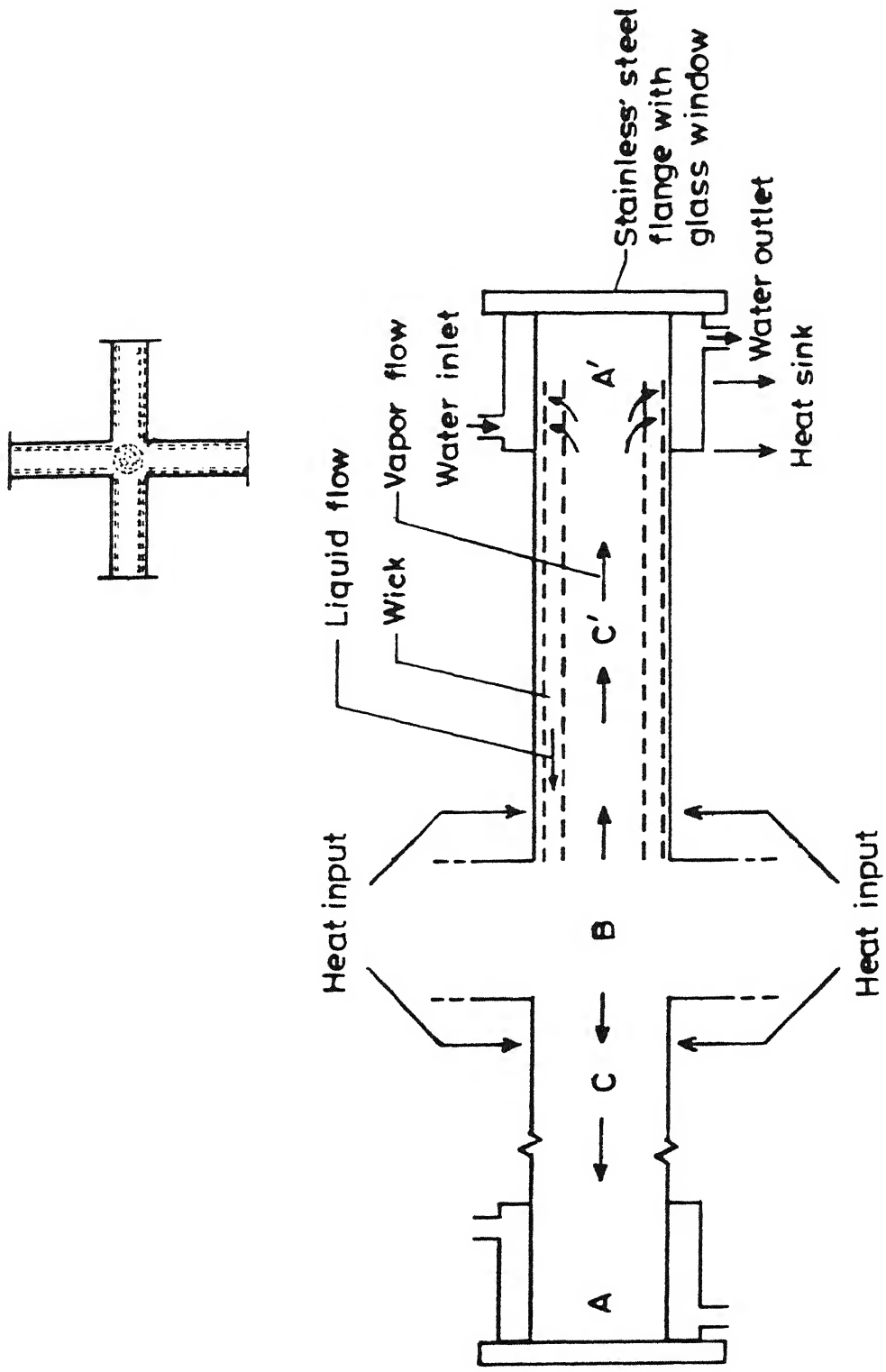

Fig. 4 Working of heat pipe. Inset shows a crossed heat pipe.

pipe of 1" diameter and 2-3 mm wall thickness. The length of each arm of the pipe was 16 cm. An annular stainless steel plate with O-ring groove was welded to each end of the pipe. Quartz windows were pressed on to the pipe by O-rings contained in the annular stainless steel flange plates. For continuous cooling, water jacket, was provided at all the four ends of the heat pipe. To start with, the heat pipe was thoroughly cleaned with HCl acid and acetone. Clean stainless steel mesh was rolled into layers and was inserted in all the four arms of the heat pipe. The heat pipe was connected to the vacuum system through copper tubing. The vacuum system consisted of a rotary pump and an oil diffusion pump giving vacuum better than 10^{-4} Torr. Gas filling arrangement consisted of a He cylinder and a glass bulb which serves as a reservoir. The bulb was first evacuated and then filled in with He at about 10 psi pressure. Heat pipe was evacuated to a pressure less than 10^{-4} Torr, and then filled with the He gas at the desired pressure. Oil manometer was used to monitor pressure. At the center of the heat pipe a heating tape was wrapped uniformly, and covered with a fire brick structure to reduce convection losses. A Chromel Alumel thermocouple was inserted from top by drilling hole in the brick structure in such a way that the thermocouple

touches the outer surface of the heat pipe at its center. The empty heat pipe (with mesh) was baked for several hours continuously at high temperature (about 500^{o}C) under vacuum. A temperature controller (Aplab, Type PTC-372) was used to fix the temperature to a desired value. The temperature variation remained within $\pm$ 5^{o}C. During this temperature variation the cadmium vapor pressure is nearly constant. Then pure cleaned cadmium metal was kept carefully at the center of the heat pipe from one window by breaking the vacuum for a very short time. Once the system was ready it was evacuated to $\leq 10^{-4}$ Torr and then filled in with He gas at a desired pressure. The metal vapor plasma was generated by focussing Nd:YAG laser radiation at the center of the heat pipe. The experimental setup used is shown in Fig. 5. The plasma was imaged on to the slit of the monochromator (HRS-2, Jobin Yvon) and the PMT (IP28, Hamamatsu) output was recorded on a strip chart recorder. The monochromator was scanned using a microprocessor scan system[59].

We have used Spectra Physics (model DCR-4G) Nd:YAG laser and its harmonics in our studies for plasma production. It delivers 1 J energy in 8.0 ns (FWHM) and 2.5 ns (FWHM) at fundamental with a repetition rate of 10 pulses per second.

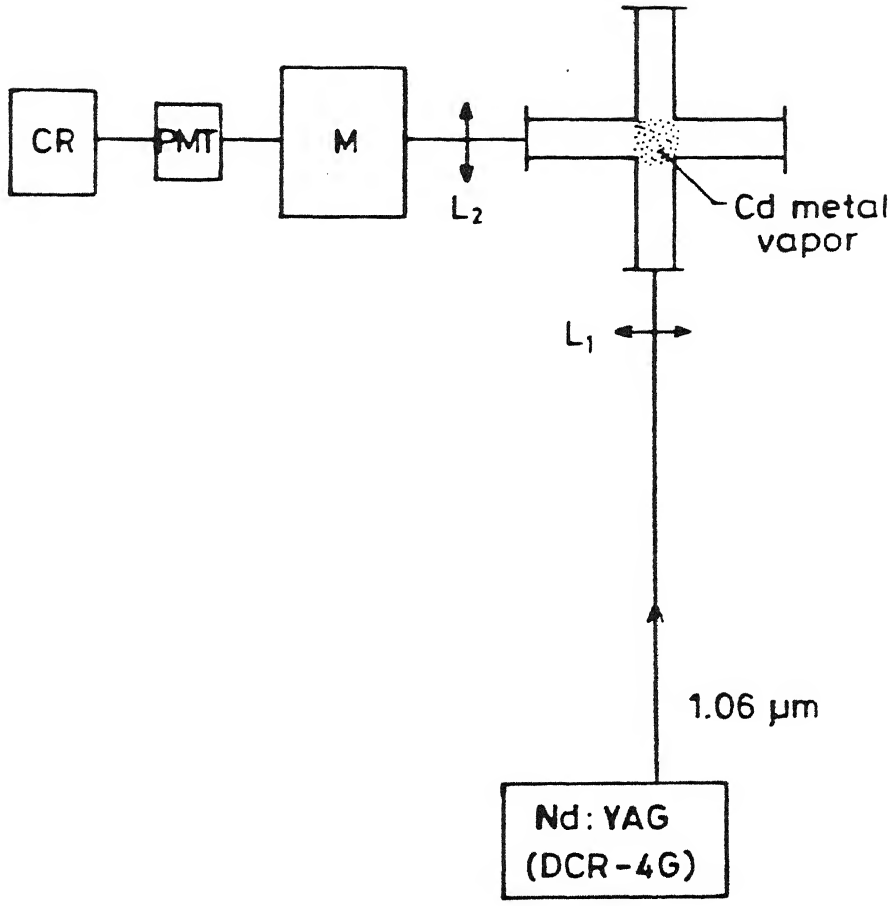

L_1, L_2-Lenses; M-Monochromator; CR-Chart recorder; PMT-Photomultiplier tube

Fig. 5 Experimental set up

The pulse width of harmonics scales as 1.06 μm pulse width devided by $\sqrt{2}$. The laser has a Gaussian limited mode structure, the beam divergence being less than 0.5 mrad. The energy of the laser was monitored using a laser power meter (Ophir Model 30 A) by placing the power meter in the path of the main beam. Laser energy was varied by varying the voltage on the laser amplifier. Burn patterns taken at different energies show no significant variation in mode pattern. The laser pulse was checked using a fast photodiode (Antel, Model AS-2, risetime < 35 ps). The output from the detector is displayed on the oscilloscope (100MHz, TS-8123 Iwatsu) with 50 Ω terminator and fed on to the boxcar averager (SRS 250) as shown in Fig. 6. Boxcar (SRS) was triggered externally with a Q switch synchronous pulse from the YAG laser. The synchronous pulse of about 8 V was attenuated to 0.8 V for triggering the boxcar averager. The average output from the boxcar averager was recorded on the strip chart recorder. A typical temporal profile of the 8.0 ns (FWHM) pulse is shown in Fig. 7; in Fig. 7(b) two peaks around the main pulse are equally spaced beats. The separation between the beats is the cavity round trip transit time. Various harmonics are generated using $KD^{*}P$ crystals. To separate the second, third and fourth harmonics

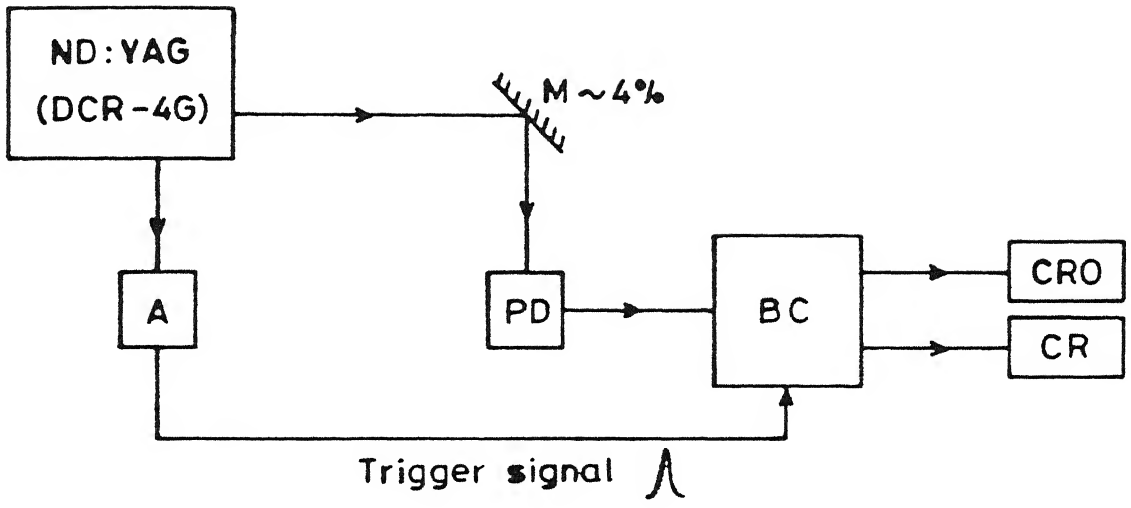

M-Mirror; A-Attenuator; PD-Photodiode; BC-Box Car averager; CRO-Storage oscilloscope; CR-Chart recorder

Fig. 6 Experimental set up for measurement of pulse width of Nd:YAG laser.

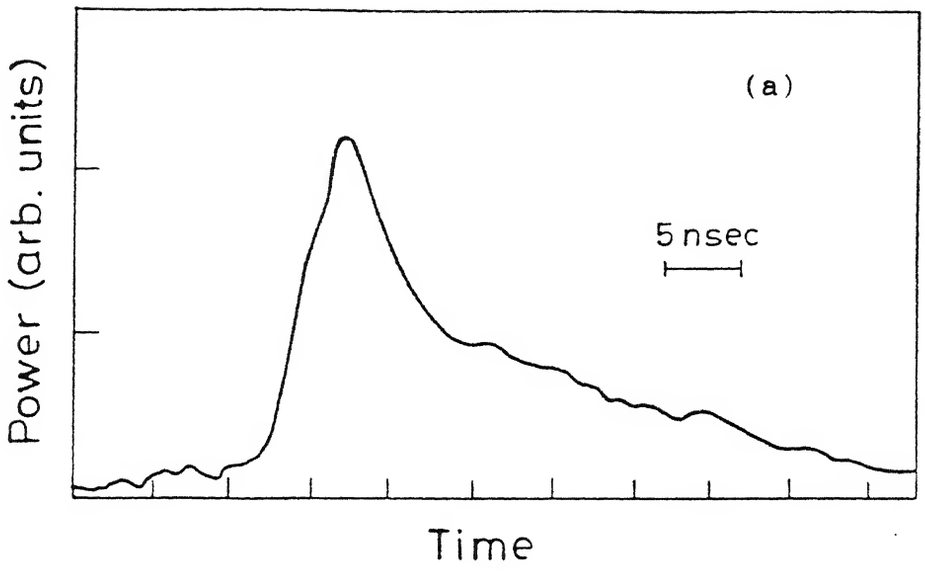

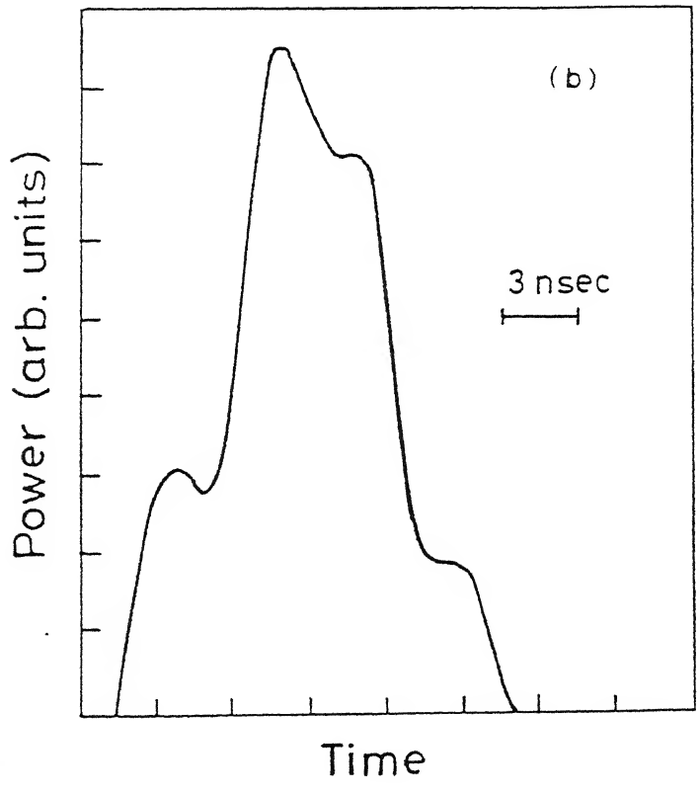

Fig. 7 Typical temporal profile of the Nd:YAG laser

(a) 1.06 μm, 8.0 nsec (FWHM)

(b) 0.532 μm, 1.8 nsec (FWHM)

from the fundamental the Prism Harmonic Separator (PHS) is used. The layout of Prism Harmonic Separator is shown in Fig. 8. To separate second harmonic (0.532 μm) from fundamental the prism P-1 is adjusted to center the incident beam on the prism P-2 and directing 0.532 μm beam through P-2 on to the output prism P-3. P-3 is then adjusted to get the output beam from the output window. In order to separate third harmonic from fundamental (1.06 μm) and second harmonic (0.532 μm),P-1 is again adjusted together with the half wave plate ($\lambda/2$) to center the 0.355 μm beam on the half wave plate. The output is taken from the output window after adjusting the output prism P-3. Fourth harmonic (0.266 μm) is separated from the other three harmonics after replacing the prisms P-1 and P-3 (or P-4) by quartz prisms. One small quartz prism P-5 acts as P-2 in directing the fourth harmonic on to the output prism P-3. Now P-3 is adjusted to center the beam onto the output window. While looking for harmonics care was taken to direct the fundamental (1.06 μm) beam on to the beam dumper.

As the laser was newly procured while the performance and other parameters of the laser were being checked, an extensive and systematic study was undertaken to investigate the effect

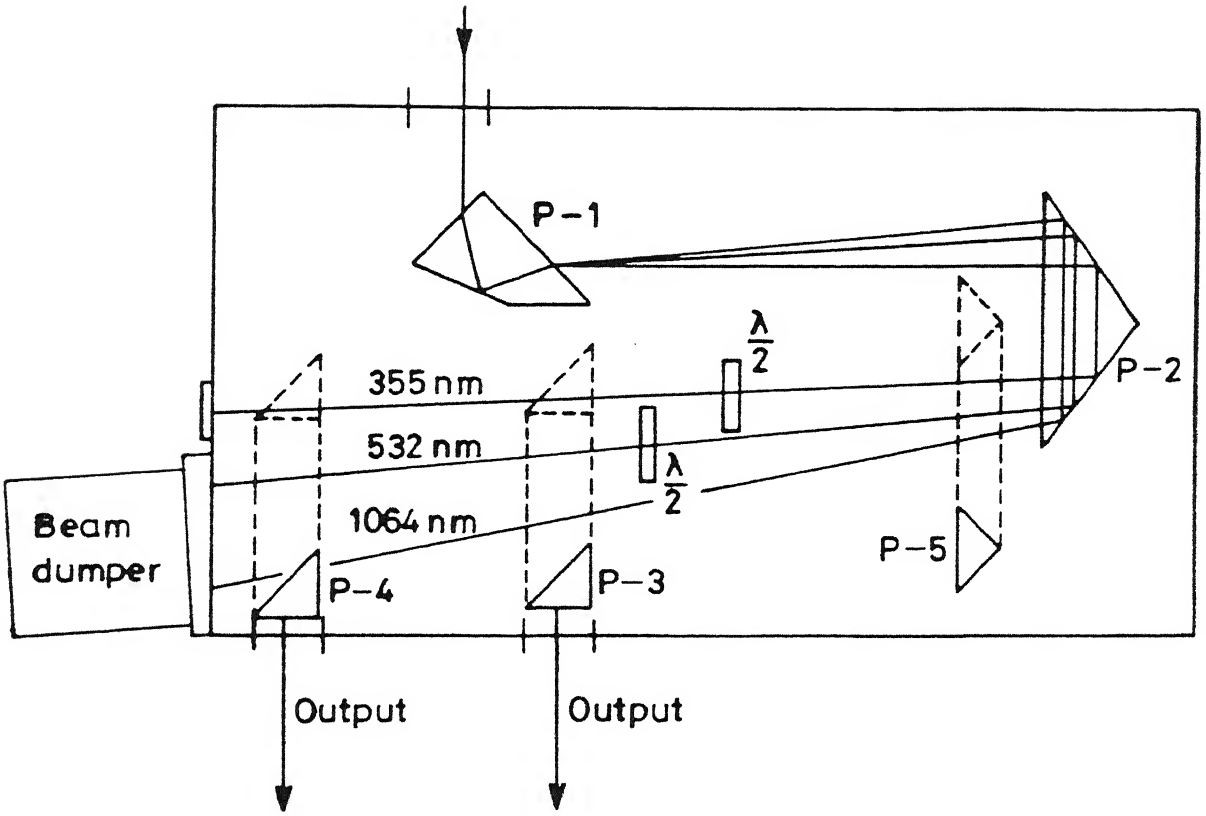

P-1, P-2, P-3, P-4, P-5 are Prisms

Fig. 8 Prism Harmonic Separator

of spot size and pulse width of laser on breakdown threshold of air, by focussing laser radiation in air with quartz lenses of f-number f/7.06, f/11.76, f/14.12, f/18.82 and f/23.52. The focal length of the lenses being between 6 and 20 cm. The laser energy was varied by varying the voltage on the laser amplifier. It is observed that the threshold intensity decreases as the focal spot size increases. Increase in threshold for smaller spot size may be due to diffusion of electrons out of the focal volume. Variation of threshold field with diffusion length shows[60] that for longer pulses (4 to 8 n sec) the effect of diffusion length is strong as compared to short duration pulses (1.3 to 2.5 n sec). We observe that the breakdown field scales with laser pulse τ_p as $\tau_p^{-0.5}$ for 0.532, 0.355 and 0.266 μm, which is in close agreement with Williams et al[61]. The threshold scales as $\tau_p^{-0.35}$ for 1.06 μm radiation similar to Van Stryland et al[62] dependence of $\tau_p^{-0.25}$. We also performed air breakdown studies in a vacuum chamber. The variation of the peak threshold intensity with pressure in the range 24-760 Torr was studied by focussing laser radiation in a vacuum chamber initially evacuated to a pressure of better than 10^{-3} Torr. We observe[63] that for 1.06 μm wavelength threshold intensity scales with

pressure as $p^{-0.8}$ showing a pronounce pressure dependence characteristic of collisional absorption. However, at 0.532 and 0.355 μm wavelength weak dependence on pressure $p^{-0.4}$ is observed indicating the occurance of multiphoton absorption. Thus for visible and shorter wavelengths, air breakdown may be initiated with multiphoton absorption and then proceed due to cascade processes.

To study tungsten plasma and a cadmium metal plasma, tungsten target was attached to a wilson seal and inserted from one arm of the heat pipe such that the target was close to the centre of the heat pipe. The laser was focussed on to the solid tungsten target from the opposite arm. To avoid crater formation, the target was slowly rotated with a small electric motor. The spectrum of the cadmium metal vapor plasma in the presence of tungsten target is recorded using the same experimental set up as shown in Fig. 5. The laser produced tungsten plasma was used as a pumping source for observing laser oscillations in cadmium on $4d^{9}5s^{2}\ {}^{2}D_{5/2} - 4d^{10}5p\ {}^{2}P_{3/2}$ transition at 441.6 nm. Two metallic brewster angled cut pipes with quartz windows were attached to the two arms of the heat pipe, opposite to the laser focus and two He-Cd laser mirrors

formed the cavity. In order to calculate the density of the plasma, Mach Zehnder Interferometer was designed. The experimental set up is shown in Fig. 21. A well collimated beam of second harmonic (0.532 μm) of the Nd:YAG laser was used as a probe. Heat pipe was kept in one arm of the interferometer. In the presence of plasma, phase difference is produced in the two beams which causes a phase shift. The interferograms were recorded on a panchromatic film using a lens less camera. By measuring the fringe shift,the plasma density n_e was calculated. The total phase difference between the two beams is given by eq. (2) as,

$$\Delta\phi = (2\pi/\lambda_p) \int_o^{r_o} (1-\mu)\, dy \qquad (2)$$

This phase difference produces a shift in the fringes equal to $\left\{N(x)/\Delta\right\}$, where N(x) is the shift produced at various distance from the target and Δ is the fringe spacing, r_o is the size of the plasma, and λ_p is the probe wavelength.

Rearranging eq (2),

$$\frac{\Delta\phi}{2\pi} = \frac{N(x)}{\Delta} = \frac{1}{\lambda_p}\int_o^{r_o}(1-\mu)\,dy$$

$$\text{or} \quad N(x) = (\Delta/\lambda_p)\int_o^{r_o}(1-\mu)\,dy \qquad (7)$$

The interferograms were analysed using Abel inversion technique. The technique is used for finding the radial dependence of a quantity $\varepsilon(r)$ eg. refractive index, emission coefficient etc. when measurements of the line integral of $\varepsilon(r)$ are made along the chords of an axially symmetric plasma or other dielectric medium. If the measured quantity is N(x) for a chord distant x from the axis as shown in Fig. 9, we have

$$N(x) = 2\int_o^{(r_o^2-x^2)^{1/2}}\varepsilon(r)\,dy \qquad (8)$$

$\varepsilon(r)$ is given by the Abel Integral[51]

$$\varepsilon(r) = -\frac{1}{\pi}\int^{r_o}\frac{N'(x)}{(x^2-r^2)^{1/2}}\,dx \qquad (9)$$

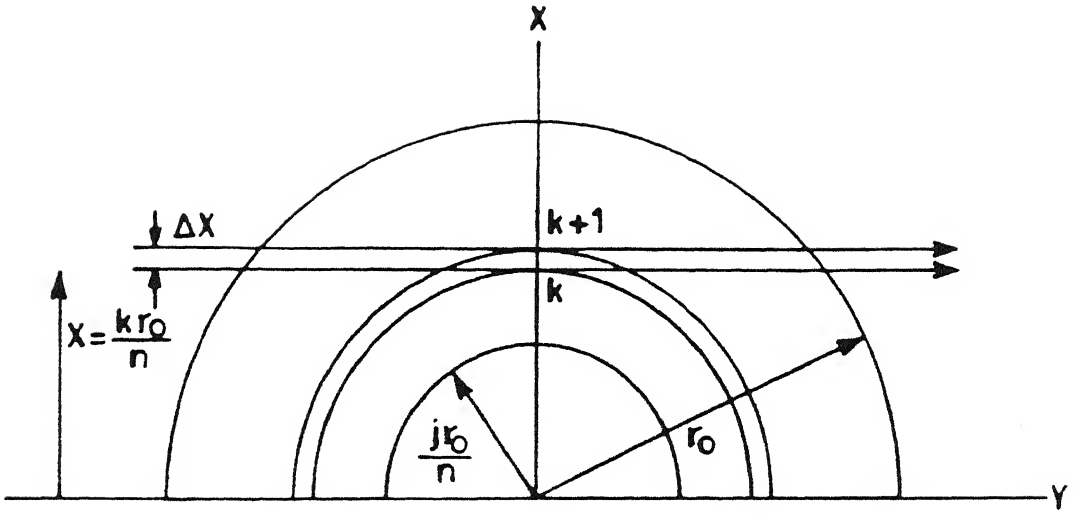

Fig. 9 Notation used for labelling the chords and radii.

The above integral is evaluated numerically with $N'(x) = \frac{\partial N}{\partial x}$ being found in some way from the experimental data[52] $N(x)$. Following Bockasten[51] the integral can be written as a series

$$\varepsilon_j = \frac{1}{r_o} \sum_{k=o}^{n-1} a_{jk} N_k \qquad (10)$$

a_{jk}'s are the Abel coefficient, r_o is the size of the plasma and N_k is the value of $N(x)$ for which $x = \left\{ \frac{kr_o}{n} \right\}$, n is the number of channels. Fig. 9 shows the plasma and different channels along which measurements are taken. The electron density can be calculated by using a 20 or 40 point cubic polynomial Abel inversion. A Computer programme was developed to calculate the Abel Coefficients and also to calculate the radial dependence of electron density.

From eqs. (3), (7) and (10), for $\omega^2 >> \nu_e^2$, we have

$$\mu = \left(1 - \frac{\omega_p^2}{\omega^2} \right)^{1/2} = 1 - \frac{\lambda_p}{\Delta} \varepsilon_j \qquad (11)$$

where ε_j's follow from eq. (10), from eq.(11) we have

$$n_e(r) = \frac{4\pi^2 m \epsilon_o c^2}{e^2 \lambda_p} \frac{1}{\Delta} \varepsilon_j \qquad (12)$$

Eq. (12) gives the radial dependence of electron density.

In order to study the dependence of plasma temperature on laser intensity and wavelength, a detailed study of laser produced aluminium plasma was undertaken in a vacuum chamber,using all the four harmonics of the Nd:YAG laser. The vacuum chamber was evacuated to a pressure of $< 10^{-3}$ Torr. To avoid crater formation on the target because of focussed laser radiation, the target was slowly rotated using a small electric motor. The plasma emission was imaged on to the monochromator slit and recorded on a chart recorder.

Assuming the plasma to be in local thermodynamic equilibrium[48] an estimate of electron temperature was made by taking the ratio of intensity of two spectral lines and using the relation[49],

$$kT_e = \frac{E' - E}{\ell n(I \lambda g' A' / I' \lambda' g A)} \qquad (13)$$

where E and E′ are the excitation energies of the upper level,

I's the intensity, λ, A, and g are respective wavelength, transition probability and statistical weight of the transition under consideration. The slope of the curve E'-E against $\ell n(I\ \lambda\ g'A'/I'\lambda'g\ A)$ gives the electron temperature. The estimated temperature lies between 0.8 and 4.0 eV.

To calculate the electron density, line profile of Al II on $4p\ ^1P_1-4d\ ^1D_2$ transition at 559.3 nm was recorded by keeping the monochromator resolution to the maximum, so that Stark width can be evaluated.

The electron density was found to be $\sim 2\times10^{16}$ cm^{-3}, using 1.06 μm laser radiation for plasma production.

CHAPTER III

LASER PRODUCED ALUMINIUM PLASMA

INTRODUCTION

By focussing a high power laser on to a solid target it is possible to get a high temperature and high density plasma[64]. The plasma characteristics depend on the laser intensity, wavelength, pulse duration and material of the target. Such plasmas are important in studies of highly ionized species[65]. Laser produced plasmas in metals in the presence of background gas have been used in the recombination phase for generation of laser oscillations[66] and as a strong x-ray and vacuum ultraviolet sources[34,67,68]. Soft x-ray emission from gold foils target has been studied[69] using 0.35, 0.53, 1.06 and 10.6 μm wavelengths to evaluate the radiation temperature and radiation conversion efficiency as functions of laser intensity and wavelength. Both emission as well as absorption spectroscopy of laser produced plasmas is very useful for evaluation of plasma parameters. Time resolved studies[70] of germanium to determine the average ionization degree and the distribution of ion stages as a function of time during the expanding, cooling phase of the plasma have been reported.

Aschkenazy et al[47] reported electron density measurement of capillary plasma based on Stark broadening of hydrogen lines. Optical spectroscopy of a plasma produced by focussing a CO_2 laser radiation on aluminium target in air have been reported by Mckay et al[71]. The enhancement of line emission from laser produced Al plasma in the presence of He, Ne, Xe and N_2 gases have been observed by Timmer et al[72]. Studies on x-ray emission from Mg plasma in the presence of H_2 and N_2 gases has been carried out by Naik et al[73]. Similar effects have been reported[74] on laser produced copper plasma in the presence of Ar gas. The effect of prepulse on x-ray production from Al plasma have been reported[75] using a 650 fsec pulse of KrF laser at 248 nm. They studied thermal and mechanical effects of laser plasma interaction to estimate total energy deposited on target and spatial distribution of the energy deposited. Theoretical studies on x-ray transmission coefficient for an Al plasma have been performed by Abdallah et al[76]. Rothenberg and Koren[77] performed studies on Al metal and alloy using 15 nsec pulse width excimer laser and explained the relative threshold intensity for plasma production in two cases. Recently studies on laser produced copper plasma in the presence of background gas using XeCl excimer laser have also

been reported[74]. A detailed study on UV, visible spectroscopy of Al plasmas have been carried out by Knudston et al[78] using a 2 μsec pulse of flash lamp pumped dye laser operated using Rh6G-dye at 583 nm.

The aim of the present work is to report the studies on the laser produced Al plasma in vacuum using Nd:YAG laser radiation and its harmonics $2\omega_o$, $3\omega_o$, $4\omega_o$. We studied the spatial variation of temperature along the axis of the expansion of plasma, produced by 0.532, 0.355 and 0.266 μm radiation. The expansion velocities of Al I, Al II and Al III ions were evaluated from the temporal profile of the emission lines. The electron density from Stark width measurement was carried out using 1.06 μm radiation for plasma production with 1J energy in 8.0 nsec (FWHM) and 2.5 nsec (FWHM) pulses. Dependence of electron temperature on intensity of 1.06 μm radiation was also studied.

EXPERIMENTAL

Schematic of the experimental set up is shown in Fig. 10. A Nd:YAG laser (DCR-4G) with Gaussian limited mode structure delivering upto 1 J of energy in 8.0 nsec (FWHM) and 2.5 nsec

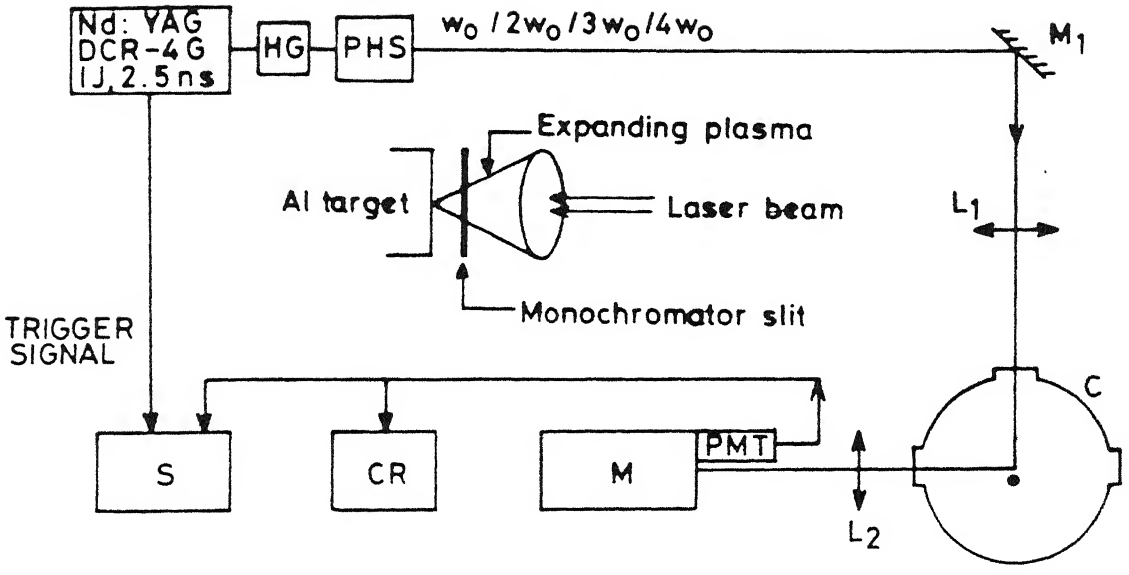

HG-Harmonic Generator; PHS-Prism Harmonic Separator; M_1-Reflecting Mirror; L_1,L_2-Lenses; C-Target Chamber; M-Monochromator; CR-Chart Recorder; S-Storage Oscilloscope Inset shows the expanding plasma as seen by the monochromator slit.

Fig. 10 Experimental set up

(FWHM) at fundamental with a repetition rate of 10 pps was used for plasma production. The pulse width for the harmonics scales as pulse width of the fundamental divided by $\sqrt{2}$. The laser has a one stage amplifier and two $KD^{*}P$ crystals are used for producing second, third and fourth harmonics. All these wavelengths are separated by using a prism harmonic separator. A 50 cm focal length lens L_1, focusses the beam on the Al target kept in a vacuum chamber, which is evacuated to a pressure of better than 10^{-3} Torr. The target rod was continuously rotated with a small external motor so that a fresh Al surface, faces the laser pulses at each time. A lens L_2 was used to image the plasma on to the entrance slit of the monochromator (HRS-2, Jobin Yvon) to get 1:1 correspondence between the size of the plasma and its image. Monochromator was continuously tuned using a microprocessor scan system. The PMT (IP28, Hamamatsu) output was recorded on a strip chart recorder or displayed on the storage oscilloscope (100 MHz, TS 8123 Iwatsu).

RESULTS AND DISCUSSIONS

The emission spectrum of Al plasma (produced by all the four wavelengths) was recorded in the visible region at

different distances from the target surface. This was done by moving the monochromator in the horizontal plane in a direction perpendicular to the axis of the lens L_2. The time integrated spectrum of the plasma produced by 0.266 μm radiation at a distance of 3 mm from the target is shown in Fig. 11(a) and (b). The aluminium emission lines were identified using the information available in the literature[79]. Fig. 11 shows many lines belonging to Al I, Al II and Al III species. Because of predominant continuum emission very close to the target it was not possible to record the spectrum close to the target. Fig. 12 shows a portion of the spectrum in the range from 550 and 580 nm at various distances from the target using 0.266 μm radiation. We observe that the intensity of Al II (559.3 nm), Al III (569.6 nm) and Al III (572.3 nm) lines decrease away from the target.

To estimate the velocity of the plasma produced by 1.06 μm radiation of pulse width 8.0 nsec (FWHM) and 0.355 μm radiation of pulse width 4.0 nsec (FWHM) radiation, we recorded the temporal profiles at different distances from the target for the transition $3p\ ^2P_{3/2} - 4s\ ^2S_{1/2}$ at 396.1 nm of Al I, transition $4p\ ^1P_1 - 4d\ ^1D_2$ at 559.3 nm of Al II and transition

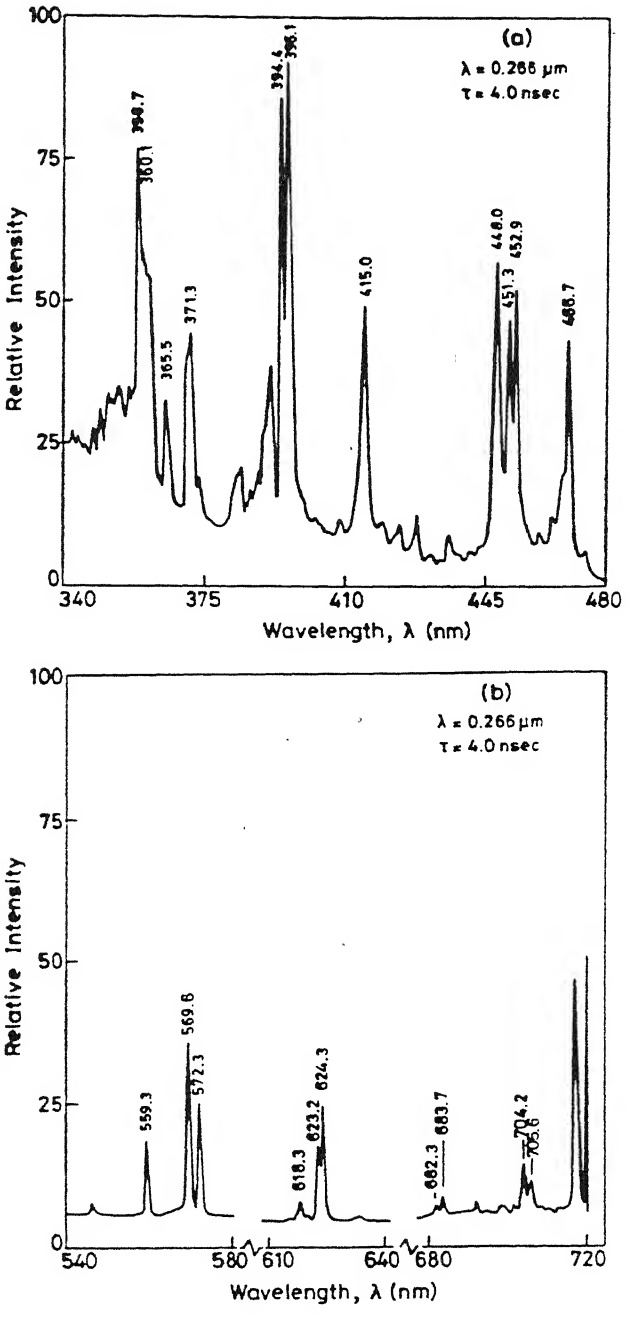

Fig. 11 Plasma emission spectrum at 3 mm from the target produced by 0.266 μm irradiation, ($I = 3 \times 10^{10}$ W/cm^2)

(a) Spectrum range 340-480 nm.

(b) Spectra range 540-580 nm; 610-640 nm;

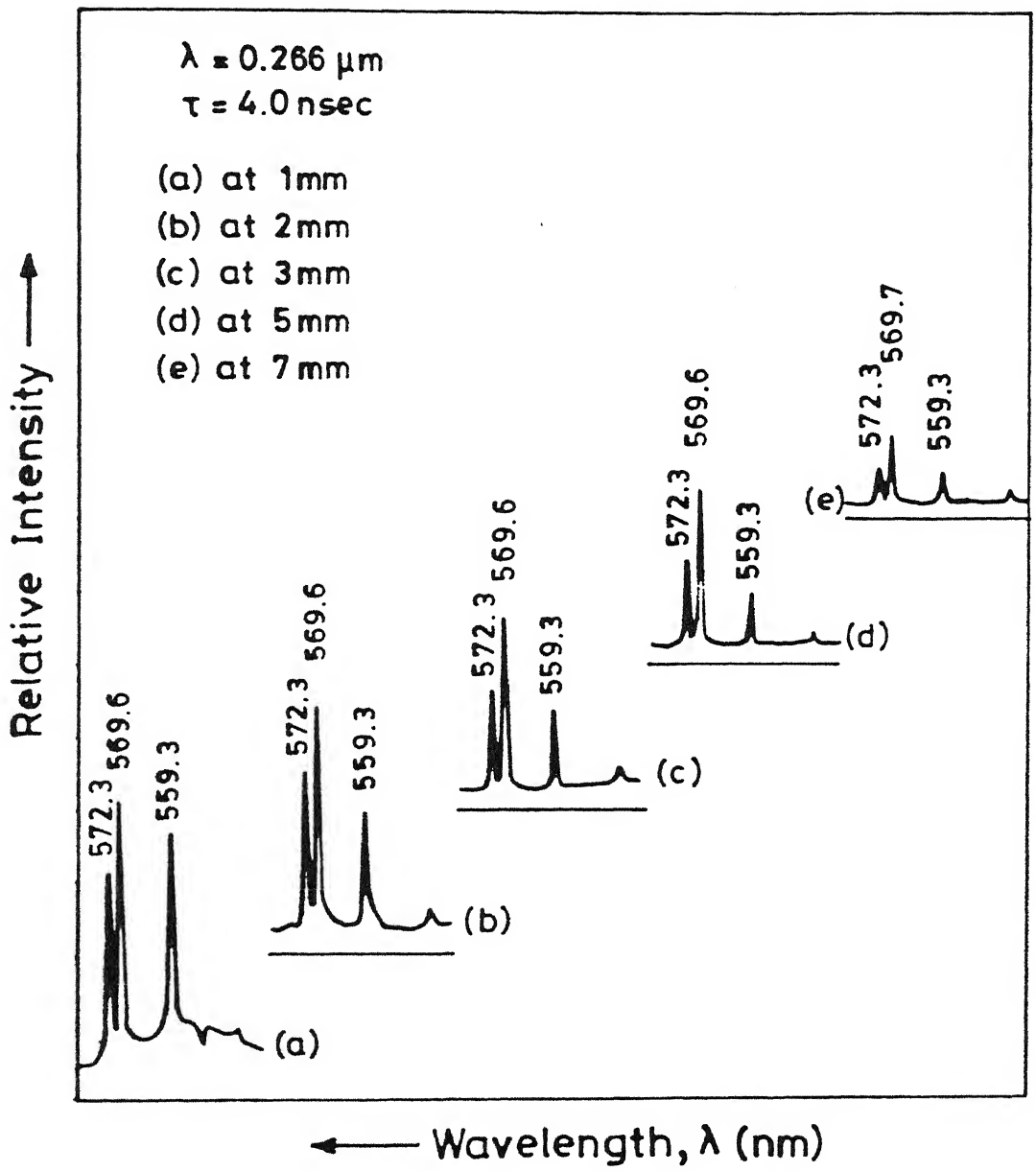

Fig. 12 Variation of intensity of Al II and Al III lines with distance from the target for 0.266 μm irradiation, ($I = 3 \times 10^{10}$ W/cm^2).

$4s\ ^2S_{1/2} - 4p\ ^2P_{3/2}$ at 569.6 nm of Al III. Fig. 13 and Fig. 14 show the variation of delay in the peak intensities with distance from the target, the slope of the curve gives the velocity of plasma front.

Assuming the plasma to be in local thermodynamic equilibrium LTE[48] the population of the bound states can be related to the electron temperature T_e by the Boltzmann distribution[48]. The electron temperature can be estimated[49] by taking ratio of intensity of two spectral lines using eq. (13). To evaluate the temperature from the recorded spectra we chose five well resolved Al II transitions. Fig. 15 shows the variation of electron temperature with distance from the target for 0.532 μm, 0.355 μm and 0.266 μm irradiation. The plasma expansion is assumed to be self regulating[80] in the sense that the density near the target equilibrates with the incident radiation. When the density is decreased radiation reaching the target surface increases causing more vaporization of the target material and consequently increasing the density. If the density exceeds the equilibrium value, the direct heating of the target is reduced and the density is decreased. It also follows from Fig. 15 that the best fitted curve gives

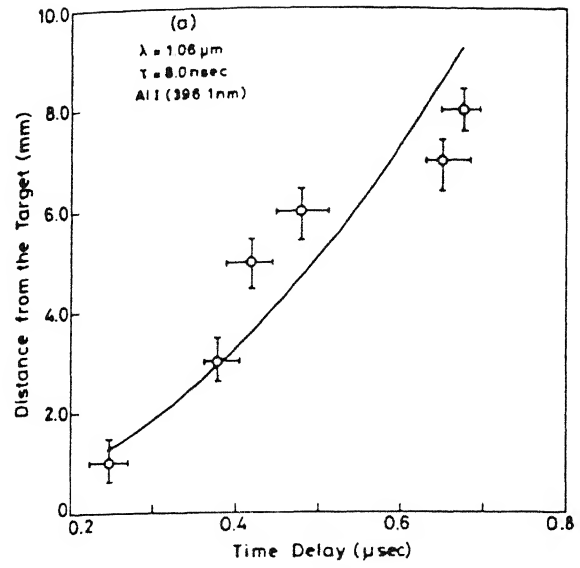

(a) Al I transition ($3p^2P_{3/2}$ - $4s\ ^2S_{1/2}$) at 396.1 nm

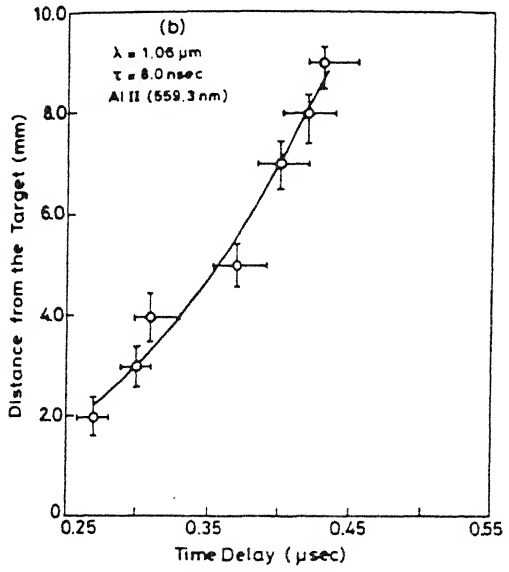

(b) Al II transition ($4p\ ^1P_1$-$4d\ ^1D_2$) at 559.3 nm

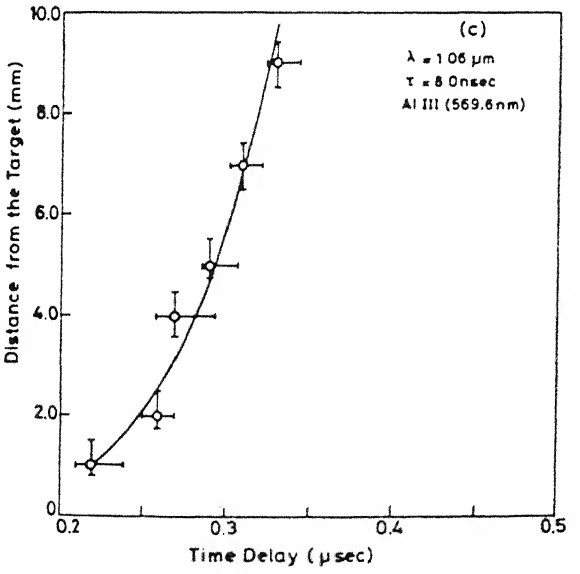

(c) Al III transition ($4s\ ^2S_{1/2}$-$4p\ ^2P_{3/2}$) at 569.6 nm.

Fig. 13 Variation of delay in the peak intensities with distance for 1.06 μm irradiation. ($I = 1.59 \times 10^{11}$ W/cm^2).

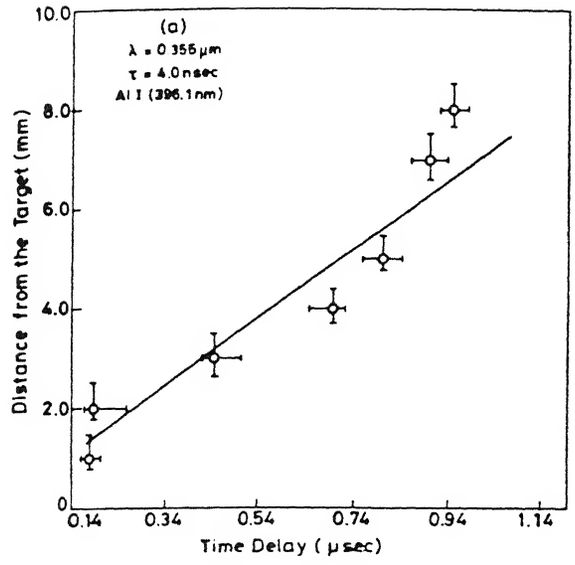

(a) Al I transition ($3p\ ^2P_{3/2} - 4s\ ^2S_{1/2}$) at 396.1 nm

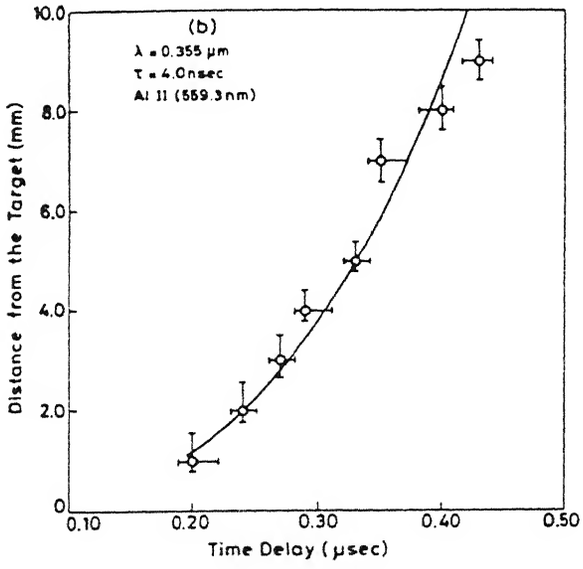

(b) Al II transition ($4p\ ^1P_1 - 4d\ ^1D_2$) at 559.3 nm

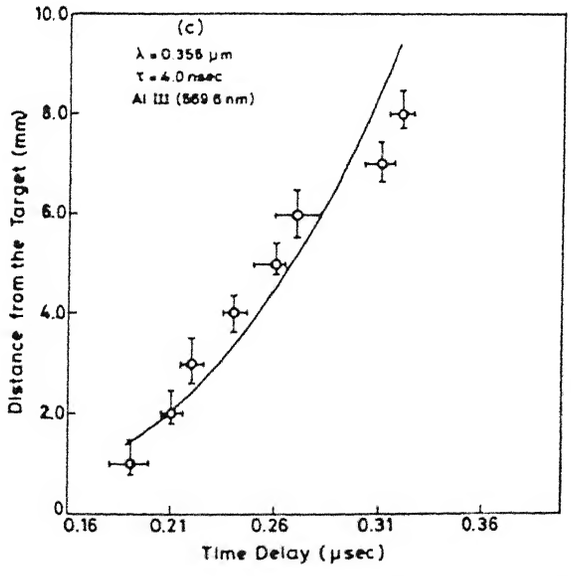

(c) Al III transition ($4s\ ^2S_{1/2} - 4p\ ^2P_{3/2}$) at 569.6 nm.

Fig. 14 Variation of delay in the peak intensities with distance for 0.355 μm irradiation ($I = 7 \times 10^{10}$ W/cm^2)

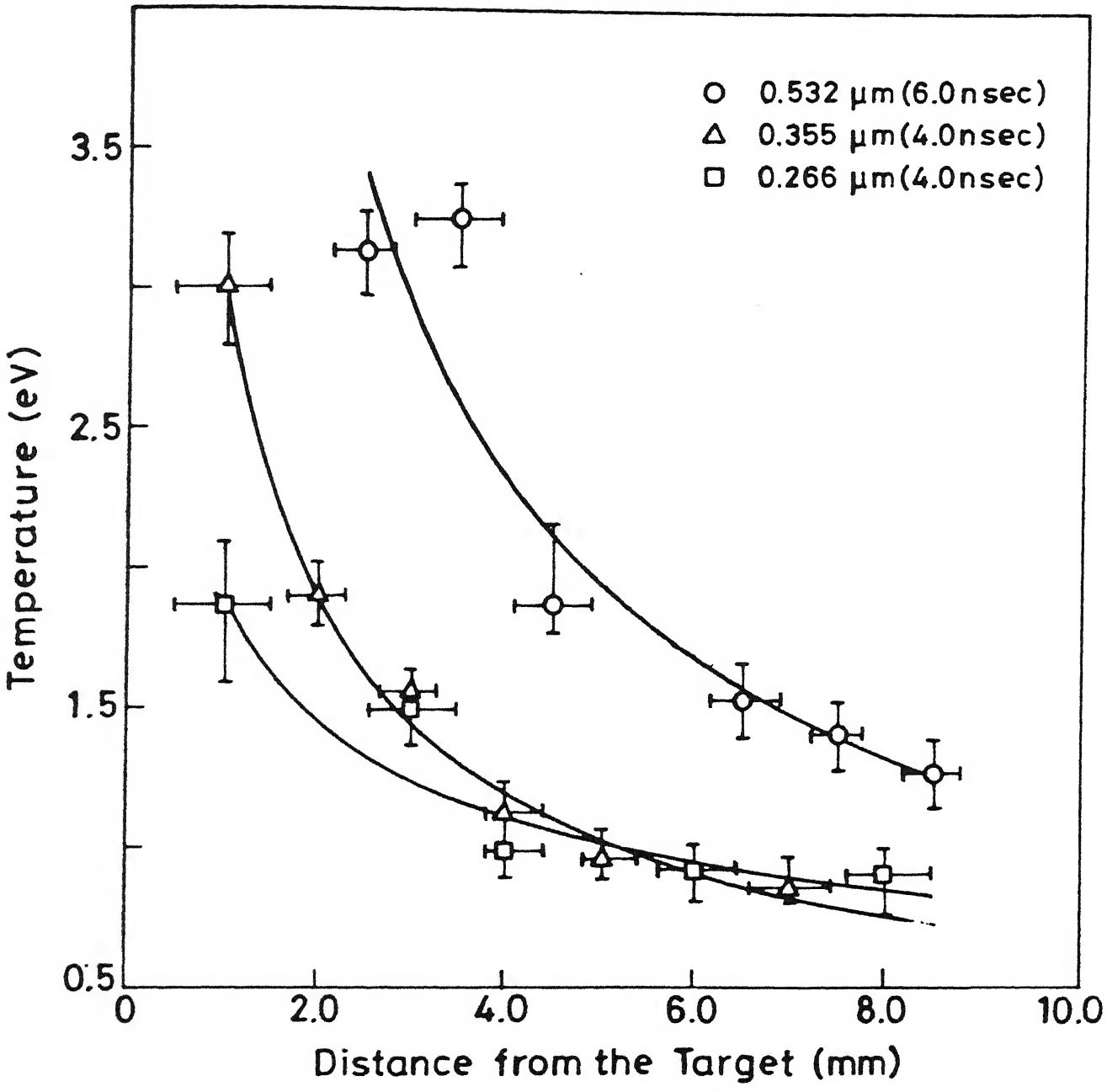

Fig. 15 Variation of electron temperature with distance from the target for various wavelengths

o 0.532 μm (6.0 nsec); I = 1×10^{11} W/cm^2

Δ 0.355 μm (4.0 nsec); I = 7×10^{10} W/cm^2

□ 0.266 μm (4.0 nsec); I = 3×10^{10} W/cm^2

$r^{-0.8}$ and $r^{-0.7}$ dependence for 0.532 and 0.355 μm wavelength respectively, where r is the distance from the target. But for 0.266 μm wavelength, $r^{-0.4}$ dependence was observed. Inverse bremmstrahlung being the dominant absorption mechanism suggests a $\lambda^{-2} T_e^{-3/2}$ scaling of absorption coefficient. The absorption coefficient is maximum in plasma close to the critical density and is given as[81]

$$K_{max} = \frac{2\pi\ Ze^2 c}{3\epsilon_o \mu} \left(\frac{m}{2\pi} \right)^{1/2} \frac{1}{\lambda^2} \left(\frac{1}{kTe} \right)^{3/2} \frac{\pi}{\sqrt{3}}\ g_c \qquad (14)$$

where g_c is the gaunt factor, given by the following expression

$$g_c(\omega, T_e) = \frac{\sqrt{3}}{\pi}\ \ell n \left[\left[\frac{2}{1.781} \right]^{5/2} \left[\frac{k_B T_e}{m} \right]^{3/2} \left[\frac{4\pi\epsilon_o m}{Ze^2 \omega} \right] \right]$$

where the symbols have their usual meanings. So the shorter wavelength light is more effectively absorbed. Fig. 16 shows the variation of electron temperature with wavelength λ at fixed laser intensity (4.0×10^{10} W/cm^2). Fig. 17 shows the dependence of electron temperature on laser intensity for wavelength 1.06 μm and pulse width 2.5 nsec (FWHM). We observe

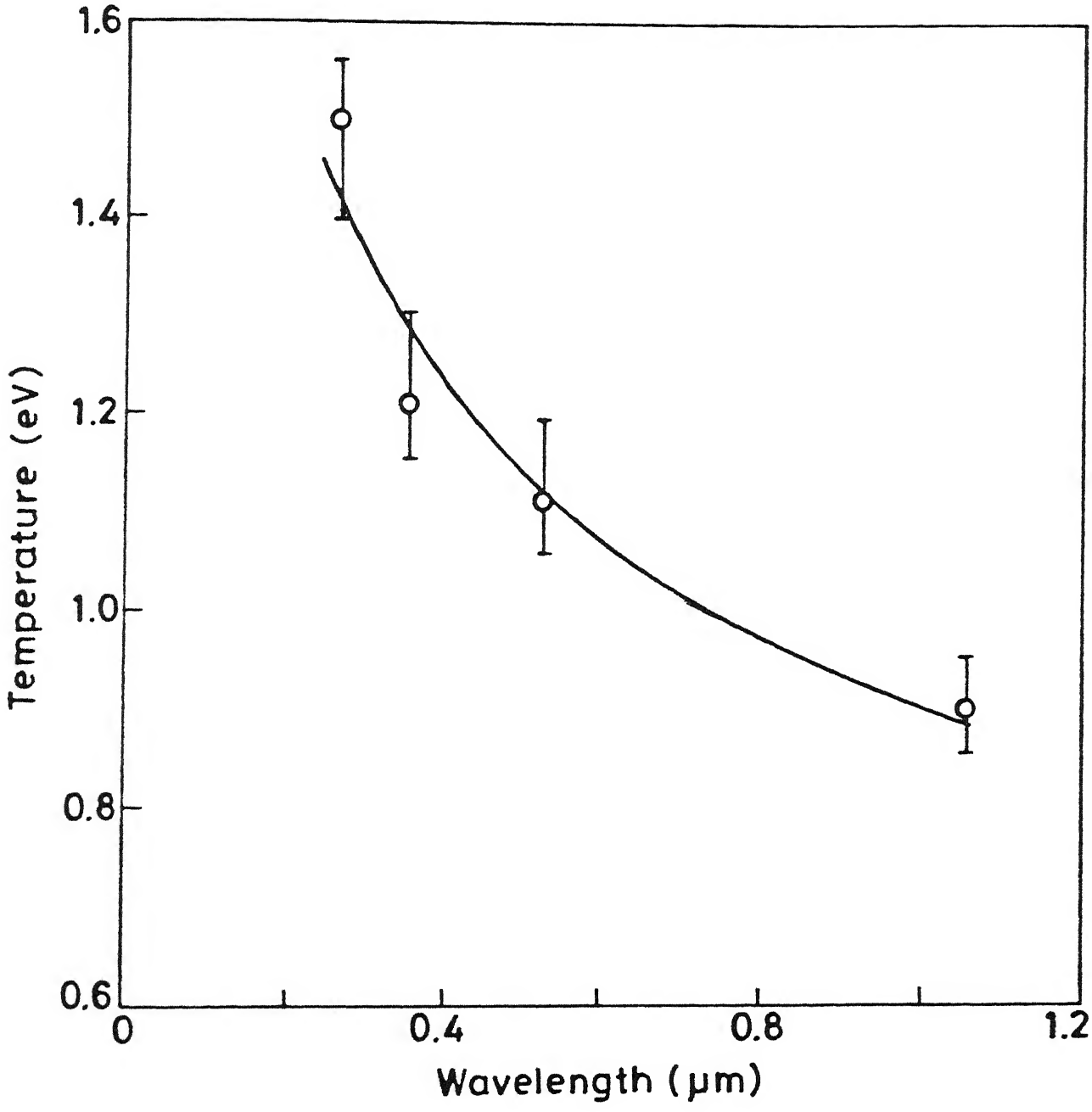

Fig. 16 Dependence of electron temperature on wavelength of incident radiation ($I = 3 \times 10^{10}$ W/cm^2).

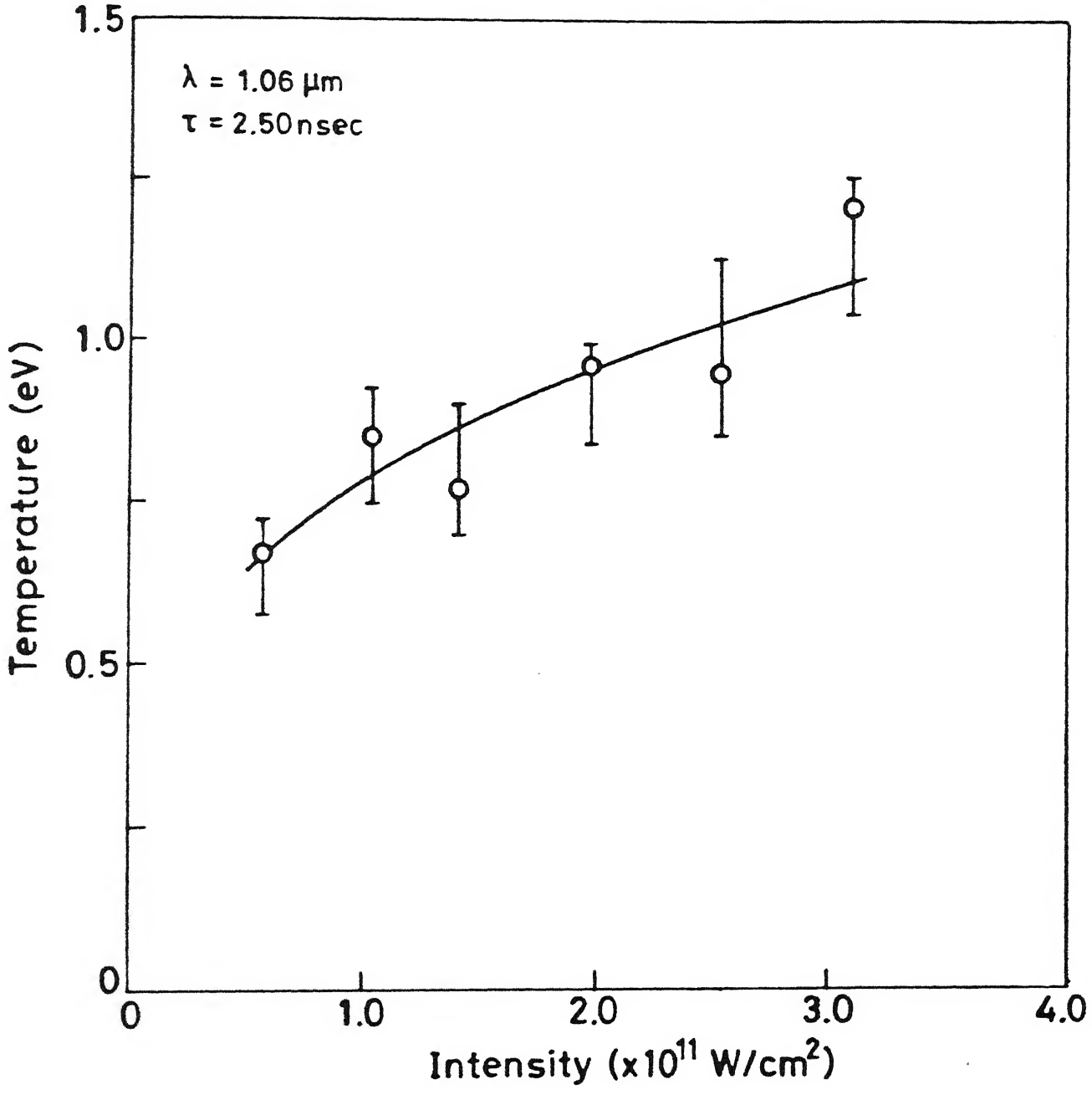

Fig. 17 Variation of electron temperature with intensity for 1.06 μm irradiation

that the temperature varies as $I^{0.3}$, consistent with the $I^{4/9}$ dependence[33] predicted from theory.

Stark broadening is due to perturbation of the energy levels of an atom or ion by the changing electric fields occurring in a collision with a charged particle. The Stark broadened line can provide the information on electron densities of plasma[82]. To estimate the electron density we recorded the line profile of Al II at 559.3 nm by keeping the monochromator resolution to the maximum (0.02 nm). The observed line is approximately Lorentzian one with the true half width $\Delta\lambda_{1/2}$ being given[82] by

$$\Delta\lambda_{true} = \Delta\lambda_{observed} - \Delta\lambda_{instrument} \qquad (15)$$

The full width at half maxima $\Delta\lambda_{1/2}$ of a line is given by[82]

$$\Delta\lambda_{1/2} = 2W\left(\frac{n_e}{10^{16}}\right) + 3.5A\left(\frac{n_e}{10^{16}}\right)^{1/4}\left[1-1.2\,N_D^{-1/3}\right]W\left(\frac{n_e}{10^{16}}\right)\ \text{Å} \qquad (16)$$

The first term in the eq. (16) gives contribution from electron broadening and the second term is the ion broadening correction; W is the electron impact parameter which can be interpolated at different temperatures[48] and A the ion

broadening parameter; both W and A are weak functions of temperature. n_e is the electron density (cm^{-3}) and N_D represents the number of particles in the Debye sphere and is given by,

$$N_D = 1.72 \times 10^9 \frac{[T(eV)]^{3/2}}{[n_e(cm^{-3})]^{1/2}}$$

Eq.(16) is valid only in the parameter range $N_D \geq 2$ and $0.05 < A\,(n_e/10^{16})^{1/4} < 0.5$. From our measured temperature of 0.8 eV and density ~$2\times 10^{16}/cm^3$, number of electron in the Debye sphere is 9. The ion broadening parameter A at 0.8 eV gives $A(n_e/10^{16})^{1/4}$ equal to 0.11. Thus using eq. (16) for density measurement is justified. Since the contribution from ion broadening is much smaller than the electronic contribution, eq. (16) reduces to,

$$\Delta\lambda_{1/2} = 2W \left[\frac{n_e}{10^{16}} \right] \text{ in } \mathring{A} \qquad (17)$$

Fig. 18 shows the Stark broadened profile of Al II (559.3 nm) line recorded on a strip chart recorder using the

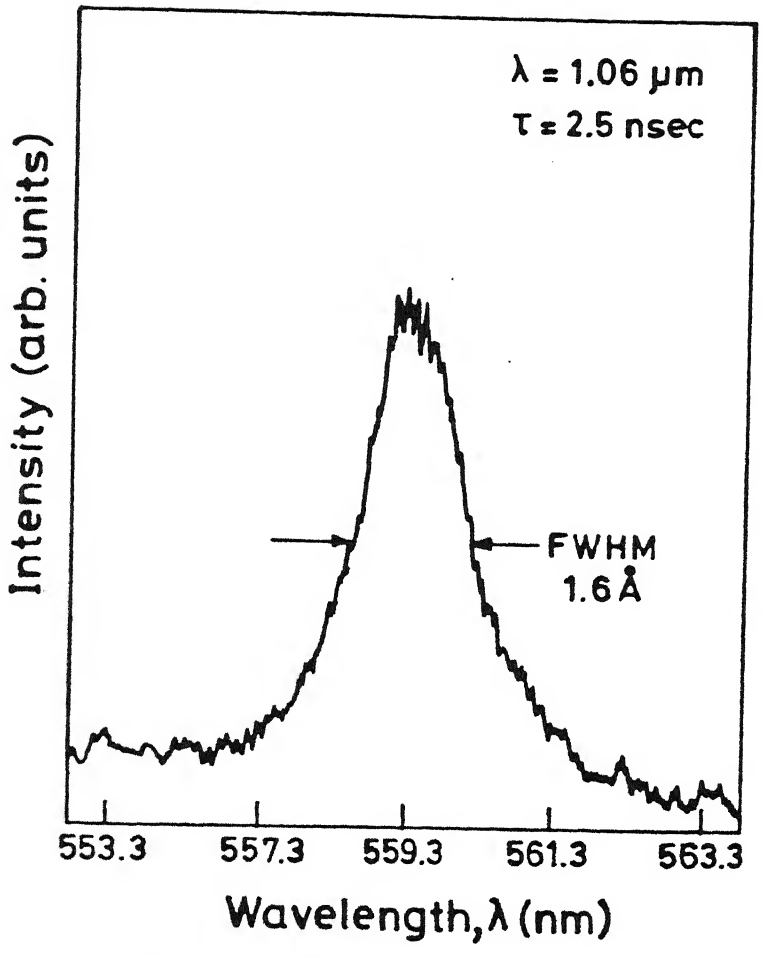

Typical Stark broadend profile of Al II (559.3 nm) line.

Fig. 18 Typical stark broadened profile of Al II (559.3 nm) line.

experimental setup shown in Fig. 10. The FWHM of the line is 1.6 Å.

Fig. 19 shows the spatial variation of electron density when 1.06 μm radiation was used for plasma production. As we move away from the target the density decreases. It follows from Fig. 19 that spatial density dependence is same for both the pulse widths used. Best fitted curve gives $r^{-0.7}$ dependence with distance from the target.

While estimating electron temperature from our data we assumed that the plasma is in local thermodynamic equilibrium. For LTE to hold, the electron-atom and electron-ion collision process must be extremely rapid and must dominate the radiative processes. So each radiative process is balanced by its inverse process. It is clear that LTE will be approached only at sufficiently large particle densities. The minimum density criterion for LTE[82] to hold is

$$n_e \geq 1.6 \times 10^{12} T_e^{1/2} (^{\circ}K) [\Delta E(eV)]^3.$$

For the transition with the largest gap (466.3 nm) $\Delta E = 2.66$ eV and highest temperature 4 eV, the lower limit for n_e is $6.47 \times 10^{15}/cm^3$. Our observed values of n_e are always greater

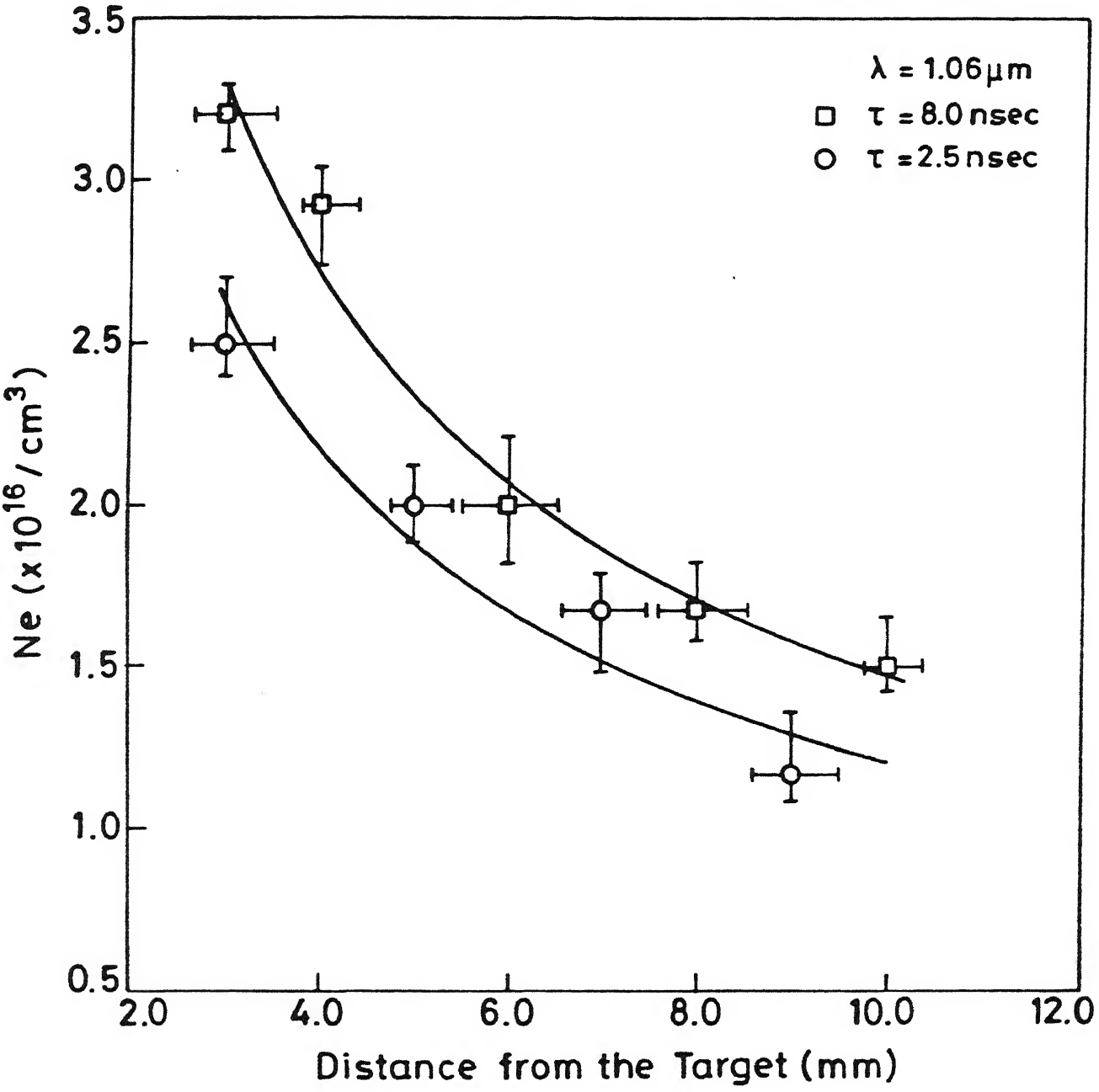

Fig. 19 Electron density as a function of distance from the target using 1.06 μm radiation.

I (τ = 8.0 nsec) = 1.59×10^{11} W/cm^2)

I (τ = 2.5 nsec) = 4×10^{11} W/cm^2

than this limit implying LTE approximation assumed for our analysis is valid.

To conclude a comparative study of laser produced Al plasma using second, third and fourth harmonic of Nd:YAG is presented. Electron temperature T_e is between 0.8 - 4.0 eV. The variation of electron temperature with intensity for 1.06 μm radiation show $I^{0.3}$ dependence on intensity. The electron temperature for same laser intensity shows $\lambda^{-0.3}$ dependence on wavelength. The electron density falls as $r^{-0.7}$ with distance from the target for both the pulse widths of 1.06 μm radiation.

CHAPTER IV

METAL VAPOR PLASMA

INTRODUCTION

Well defined homogeneous metal vapors with precise information of density and temperature needed for spectroscopic applications are generally generated using heat pipe oven[83]. The metal vapor inert gas mixtures have extensively been used in non linear optics for generation of tunable narrow band coherent light sources[84] in UV and VUV [85] region of spectrum where non linear crystals can not be used[86]. Recently, heat pipe oven have been used for production of a soft x-ray source[5,87] which subsequently pumps the surrounding metal vapors for short wavelength lasers. Spectroscopic measurements of the vapor flow velocities in Li_2 molecule as a function of pressure was studied by Vidal[56] in a heat pipe. Recently Tunnermann et al[88] have developed single shot autocorrelator for KrF (248 nm) subpicosecond laser pulses of 350 fs (FWHM) by exciting Cd vapors in a heat pipe at λ = 508 nm with a pulsed KrF excimer laser. Electron density and temperature measurement in Cs vapor plasmas using 308 nm XeCl laser have been carried out by Gawlik et al[58]. Time resolved excitation

and ionization studies of Ba vapor using a 1 μs dye laser beam tuned to 553.5 nm, have been performed by Jahreiss et al[39]. Hessel et al[89] have developed rotating type heat pipe oven which uses centrifugal force as a return mechanism for the condensed vapors in contrast to capillary return forces for the conventional heat pipe. They used the heat pipe for the studies of sodium and indium vapors. Studies[90] on Mie scattering from aerosol medium have been carried out in a heat pipe by laser evaporation of copper metal followed by sudden cooling of this vapor in either H_2, N_2 or Ar gas. We report on the studies of cadmium plasma produced using a Nd:YAG laser with and without a background laser produced plasma for pumping the Cd-vapors in a crossed heat pipe[42]. Cluster formation of Cd was also observed in the overheated heat pipe.

EXPERIMENTAL

The design and construction details of the heat pipe used in our studies has already been discussed in Chapter II. The crossed heat pipe used is a 1" diameter stainless steel pipe, a stainless steel rolled wire mesh is put in all of the four arms. The central zone was heated using a heating tape wrapped around the pipe and a fire brick structure covered the heated

zone to reduce convection losses. Once heated the liquid evaporates, to avoid deposition of vapors on the windows, water jacket is provided for cooling at each end of the four arms.

To study the effect on efficiency of getting metal vapor plasma in presence of background plasma, a high Z metal target, tungsten, was inserted in one of the arms, opposite to the direction of the incident laser beam. The plasma was observed by focussing, using a 18 cm focal length quartz lens, radiation from a Nd:YAG laser onto tungsten target for tungsten plasma and at the centre of heat pipe for metal vapors. We have used a Nd:YAG laser (DCR-4G Spectra physics) with Gaussian limited mode structure and its harmonics $2\omega_o$, $3\omega_o$, $4\omega_o$ delivering upto 1 J in 2.5 nsec (FWHM) at fundamental with a repetition rate of 10 pps. In order to expose a fresh surface of the target to the laser pulses the target was continuously rotated with a small electric motor. The other two arms of the heat pipe were used for viewing and recording of emission from plasma. The plasma was imaged on to the slit of the monochromator (HRS-2, Jobin Yvon) and detected using a photomultiplier tube (IP-28, Hamamatsu). The signal from PMT was fed to a strip chart recorder. The experimental set up is same as shown in Fig. 5.

RESULTS AND DISCUSSION

We studied, the metal vapor plasma, with and without the background high Z plasma. In the first part of our study, we concentrated on the laser produced cadmium plasma in the heat pipe. To start with the system was baked for several hours. To avoid any metal deposition on windows, water is flown continuously in water jacket at the end of each arm. Once the system is ready it was evacuated to a pressure of $\leq 10^{-4}$ Torr and then filled in with helium at required pressure. The temperature was slowly raised to 450° C with He gas pressure of 7 Torr. The laser beam was focussed at the centre of the heat pipe using a quartz lens, no cadmium plasma was observed visually. However, when the buffer gas pressure was increased to 52 Torr and the temperature was kept at 400° C a weak cadmium plasma was observed. Increasing temperature further at the same buffer gas pressure, increases the intensity of the plasma. An intense green ball of cadmium plasma was visually visible when the heat pipe was operated at 500° C, the corresponding Cd density being $2.78 \times 10^{17}/cm^3$. Fig 20 shows a Cd spectrum at oven temperature of 500° C at a He pressure of 52 Torr and laser energy 900 mJ in 8 nsec pulse, recorded using a

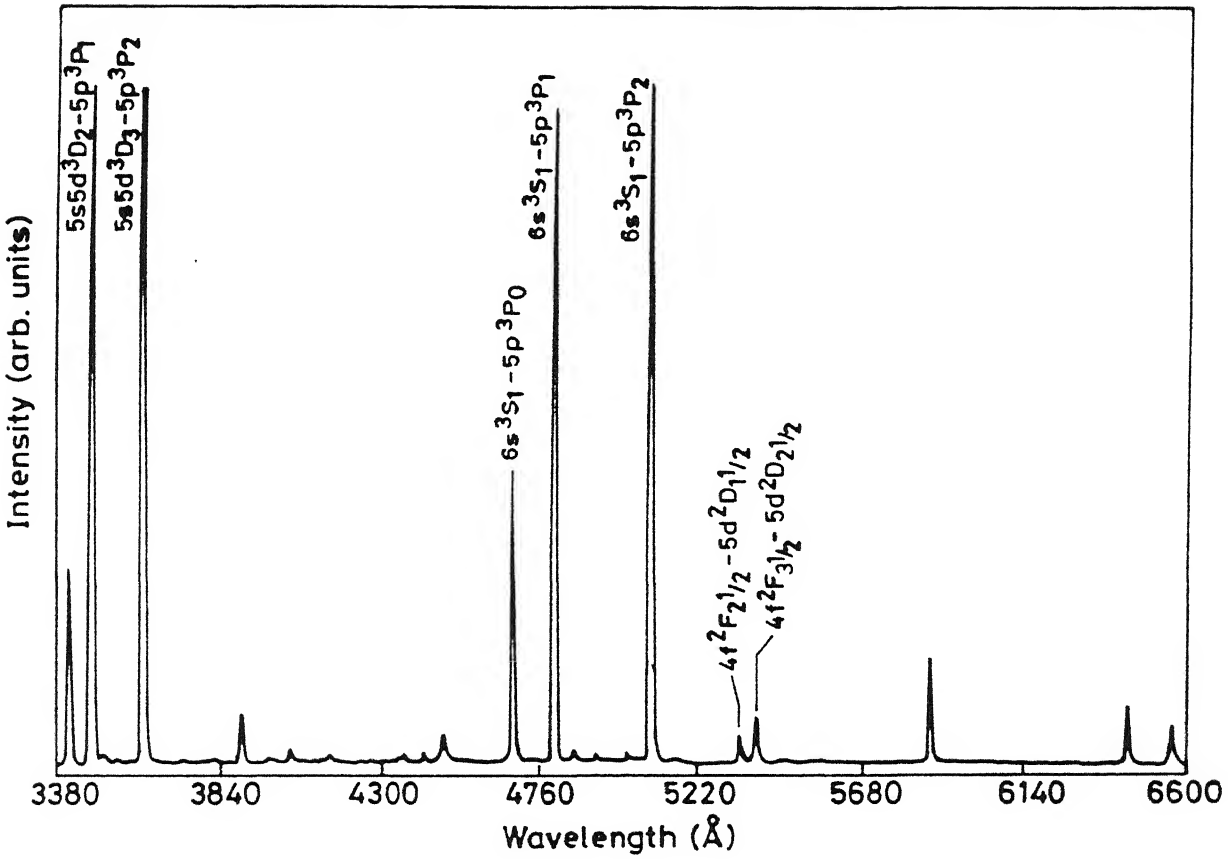

Fig. 20 Visible spectrum of Cd metal vapor plasma at a He pressure of 52 Torr.

monochromator setup as shown in Fig. 5. An estimate of the temperature of metal vapor plasma was made by taking ratio of the intensities of the spectral lines[49]. The observed temperature is 0.5 ev. The increase in the He gas pressure decreases the intensity of the emitted cadmium lines. It was also observed that the increase in temperature beyond 500^{o} C decreases the intensity of the green blob. This may be due to particulate formation[58,91], the so called 'fogging' in the heat pipe. To confirm and visually observe the formation of clusters, a weak He-Ne laser beam was sent close to the centre of the heat pipe. The pattern in transmitted laser beam was observed on a wall, about 4 m away from the heat pipe. The convective movement of the dust like particles was clearly visible in the beam. We feel that this particulate formation is due to cadmium clusters created by condensation of the metal vapors in the cold zone at the boundary with the buffer gas. Similar effect was also observed if the central part of the heat pipe is suddenly overheated. Thus the poor conditions of operation for the heat pipe, result in cluster formation of the metal. Obtaining, a high Cd density required for efficient plasma production appears to be the most difficult technical problem in the experiments, such as ours.

Our experience shows that the temperature of the heat pipe should be increased very slowly and should not exceed the value at which the vapor pressure of the metal vapor and buffer gas pressure equalise.

Second part of our studies was aimed at the possibility of using laser produced plasma as a pumping source for photo-ionization Cd^+ laser oscillating at 441.6 nm[5]. A tungsten target fixed to a rod was inserted into one of the arms of the heat pipe. It is known that by focussing the laser radiation to a small area on to solid target it is possible to create a high temperature high density recombining plasma. Near the surface of the target, the plasma emission is primarily due to free bound and to line radiation. However, for high Z target continuum radiation dominates[32] over the line radiation. The broad band emission can be approximated to a blackbody with the same characteristic temperature as that of the plasma.

In order to study coupling between background plasma and Cd plasma, the laser radiation was focussed to a spot of 100 μm on to the tungsten target with helium gas at a pressure of 7 Torr. No heating of the heat pipe was done. A bluish white plasma of tungsten was visually seen at the target

surface. The density of the laser produced plasma was estimated using a Mach Zehnder Interferometer[37]. The experimental lay out is shown in Fig. 21. A $2\omega_o$ (0.532 μm) radiation was used as a probe beam. The collimated probe beam was split into two beams of equal intensity at beam splitter BS_1 and were recombined at the beam splitter BS_2. The heat pipe was placed in one arm and a compensating glass plate was placed in the other arm of the interferometer. The interferograms were recorded on a panchromatic film using a lens less camera. The interferograms were enlarged, digitized, and analysed for fringe shift and density evaluation. Assuming the cylindrical symmetry around the central axis of the expanding plasma, the electron density can be calculated at various distances from the target surface by using Abel inversion[51] as discussed in Chapter II. Figs, 22(a) and 22(b) show the radial density distribution at a distance of 2 mm and 3 mm respectively from the target. The delay between the 1.06 μm beam and the probe beam was 19 nsec. This was the optimum value of the delay. For lower values the plasma expansion was very fast and the fringes close to the target were quickly merged. While for higher value of delays the shift was very small.

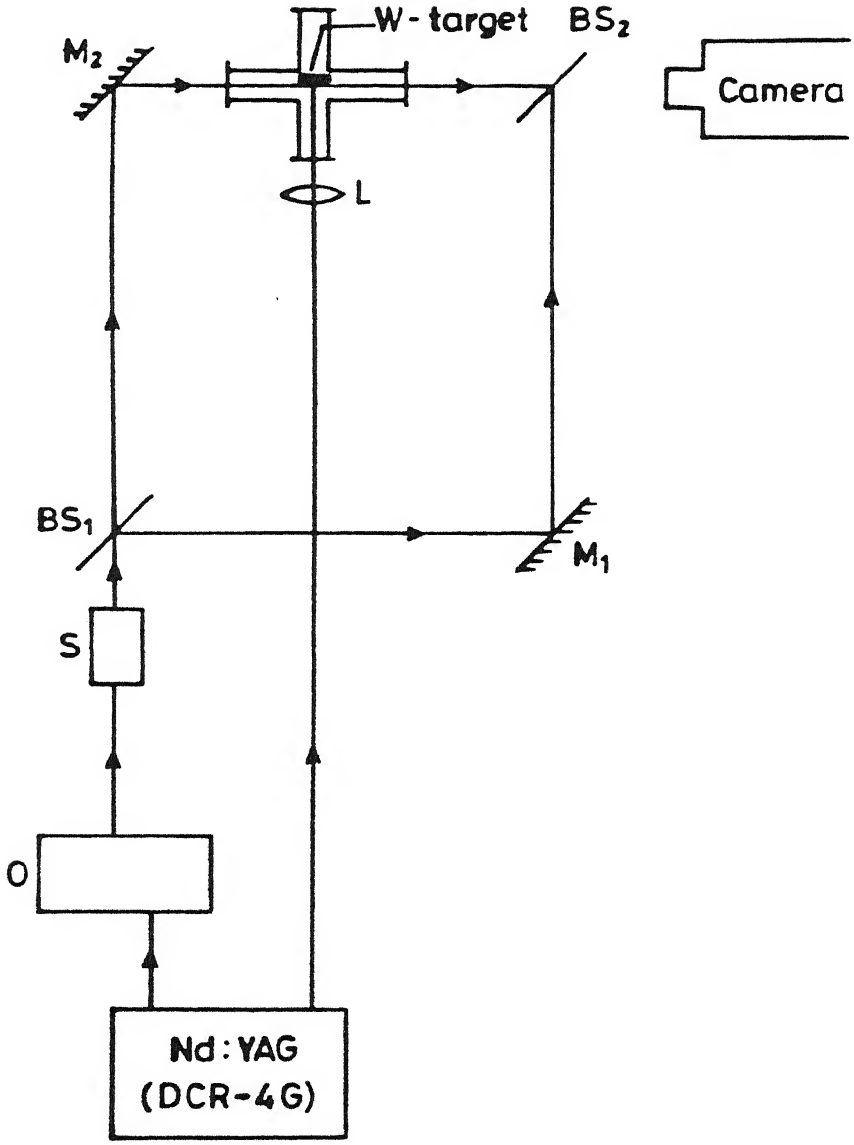

M_1,M_2-Reflecting Mirror; BS_1,BS_2-Beam Splitter;
O-Optical Delay; S-Spatial Filter and Collimator; L-Lens

Fig. 21 Measurement of electron density by Mach Zehnder Interferometer.

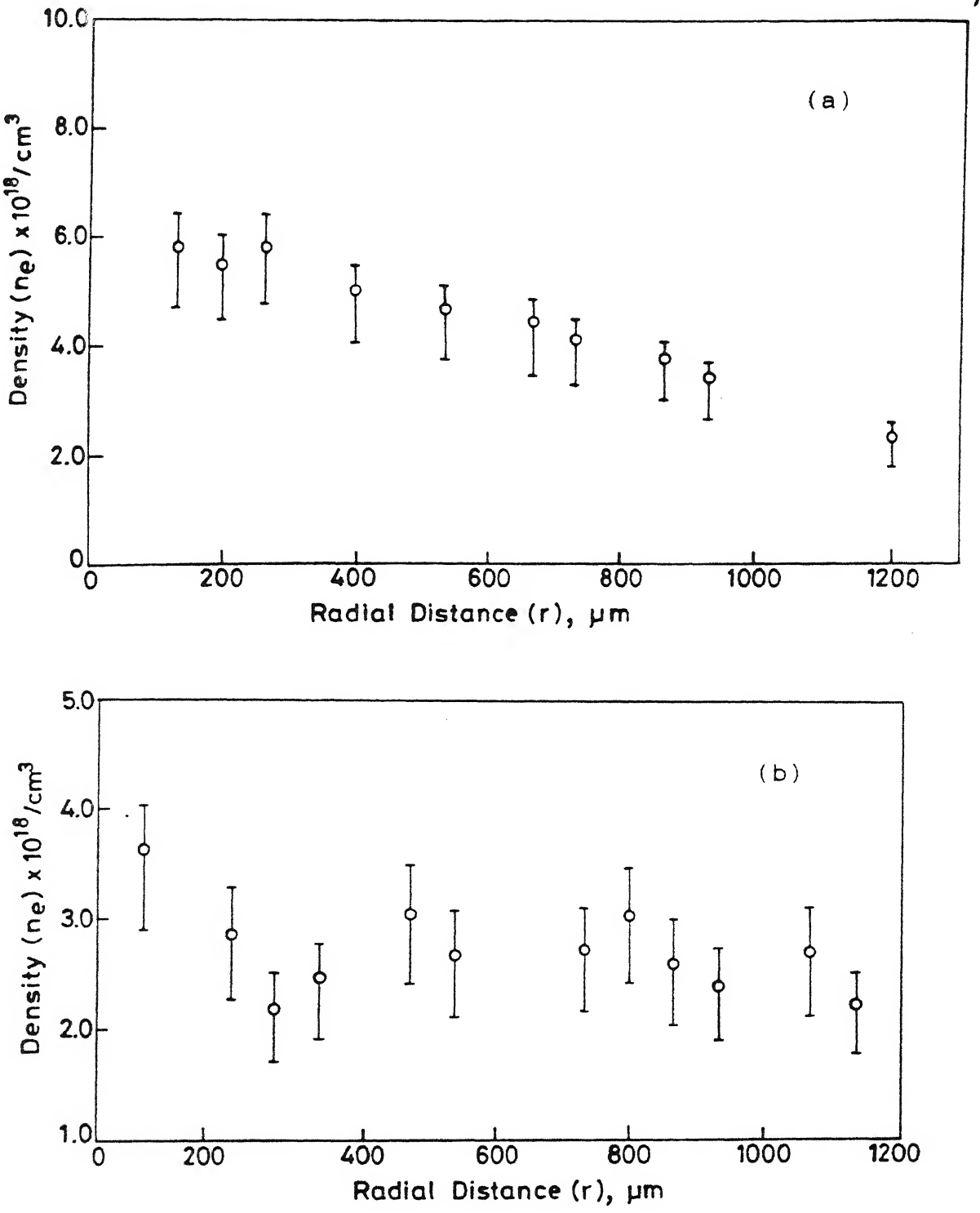

Fig. 22 Radial density profile using 1.06 μm radiation ($I = 4.7 \times 10^{11}$ W/cm^2).

(a) at 2 mm from the tungsten target surface

(b) at 3 mm from the tungsten target surface

In order to photoionize the cadmium metal vapor, the heat pipe temperature was raised to 420^0 C with a He pressure of 7 Torr and the laser radiation was focussed on to the tungsten target. We observe a bluish white plasma very close to the target surface and green plasma due to cadmium vapor extending upto 8 mm away from the tungsten surface. No Cd plasma was observed when the heat pipe was not heated. The Cd plasma was imaged onto a slit of the monochromator, Fig. 23 shows Cd spectra recorded at 4 mm away from tungsten surface. The He pressure was about 7 Torr and laser energy was 900 mJ. On comparing the two spectra (Fig. 20 and 23) we observe that the intensity of all lines increase drastically (sensitivity in Fig. 20 is five times more than that of Fig. 23) and Cd II lines which were absent in Fig. 20 are also observed in Fig. 23. Thus laser produced plasma can be a very effective source for getting higher ionic states. We estimate temperature of Cd plasma at 4 mm away from the surface of the target to be 0.3 eV. Laser oscillations on $4d^9 5s^2\ ^2D_{5/2}$ — $4d^{10} 5p\ ^2P_{3/2}$ transition at 441.6 nm were also observed.

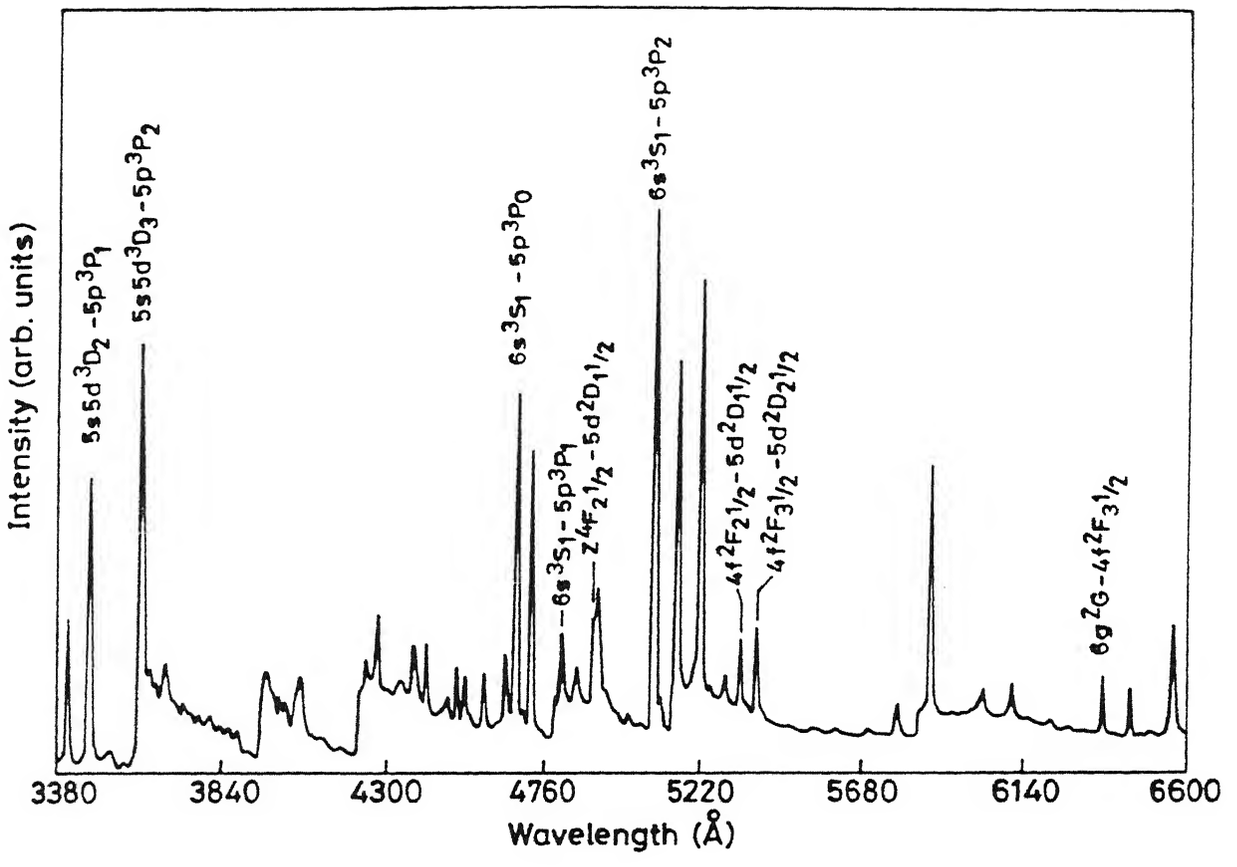

Fig. 23 Visible spectrum of Cd metal vapor plasma in the presence of tungsten plasma at a He pressure of 7 Torr.

In conclusion we studied the Cd metal vapor plasma in a heat pipe. Cluster formation was observed when the heat pipe was overheated. To study the effect of blackbody pumping, Cd metal plasma was studied in the presence of tungsten plasma. Intensity of the emitted lines from metal plasma was more in the presence of the background tungsten plasma.

CHAPTER V

CADMIUM PHOTO-IONIZATION LASER

INTRODUCTION

Chapter I describes the various mechanism to observe short wavelength lasers. Duguay et al[1] and McGuire[93] were the first to propose x-ray photo-ionization pumping for short wavelength lasers and Auger pumped short wave length lasers. Since the lifetime of the proposed upper laser levels was short Duguay et al suggested the use of short pulses and hence high peak power for producing x-rays. In order to reduce the pumping requirement, Mani et al[94] suggested of producing metastable ions. Harris et al[95] proposed the transfer of energy from Li^+ metastable levels to potential laser levels in neutral Li, lying well above the ionization energy by resonance pumping with an efficient tunable antistokes Raman source. The laser produced plasmas as x-ray sources for the excitation of XUV laser has been examined extensively and theoretically[93,96]. However, the progress on experimental investigations were slow due to complexity and inconvenience of a geometry for separating the x-ray source region from the region to be

pumped. Caro et al[97] were the first to propose that the x-ray pumping be produced within the volume of the region to be pumped. They produced Li^+ metastable by inner shell photo-ionization of neutral Li by means of soft x-rays emitted from laser produced Ta plasma. They used Nd:YAG laser for producing Ta plasma and observed metastable density as high as $6x10^{14}$ ions/cm^3 a few mm away from Ta target. Using the similar set-up Silfvast et al[3] were the first to report photo-ionization at 441.6 and 325 nm in Cd. They used a Nd:YAG laser produced Ta plasma as a source of soft x-rays for pumping Cd vapors. Using the similar configurations and pumping scheme gain measurements[5,8] on Zn^+, In^{++} and Xe^{++} are also reported. Photo-ionization laser in Cs vapor[7] has also been reported. Weigold and Piper[10] have proposed a magnesium photo-ionization laser at 24.7 nm. By focussing a high power laser onto a solid target it is possible to get a high temperature and high density plasma[64]. The plasma consists of line as well as continuum emission. It has been shown that for high intensity the XUV continuum emission dominates[32] over line radiation. The spectral distribution close to the surface of the target can be approximated by a black body radiation distribution with temperature equal to plasma. We have used a laser produced

tungsten plasma as a black body pumping source to pump cadmium vapors in a heat pipe. The laser oscillations were observed on $4d^9\ 5s^2\ ^2D_{5/2} - 4d^{10}\ 5p\ ^2P_{3/2}$ transition at 441.6 nm. The energy level diagram for cadmium photo-ionization laser is shown in Fig. 24. The x-ray flux directly populates the upper laser level from the ground level. The population inversion occurs between the $4d^9\ 5s^2$ state and $4d^{10}5p$ state. The photo- ionization cross section curve for cadmium is shown in Fig. 25. It follows from the figure that the cross section for removing the inner shell d electron begins at 18 eV rising to a maxima at 40 eV and then falls in the region of 120 eV. Because of the broad nature of the photo-ionization cross section, for efficient pumping the pumping source should also have a broad spectrum. Since the peak of photo-ionization cross section of Cd ($4d^9 5s^2$ state) is at 40 eV which corresponds to a wavelength of $\lambda \approx 300$ Å, from Wein's law it follows that the black body which is used as a pumping source should have a temperature of 8 eV. Fig. 25 shows an 8 eV black body source matched with the photo-ionization cross section of Cd ($4d^9\ 5s^2$ state).

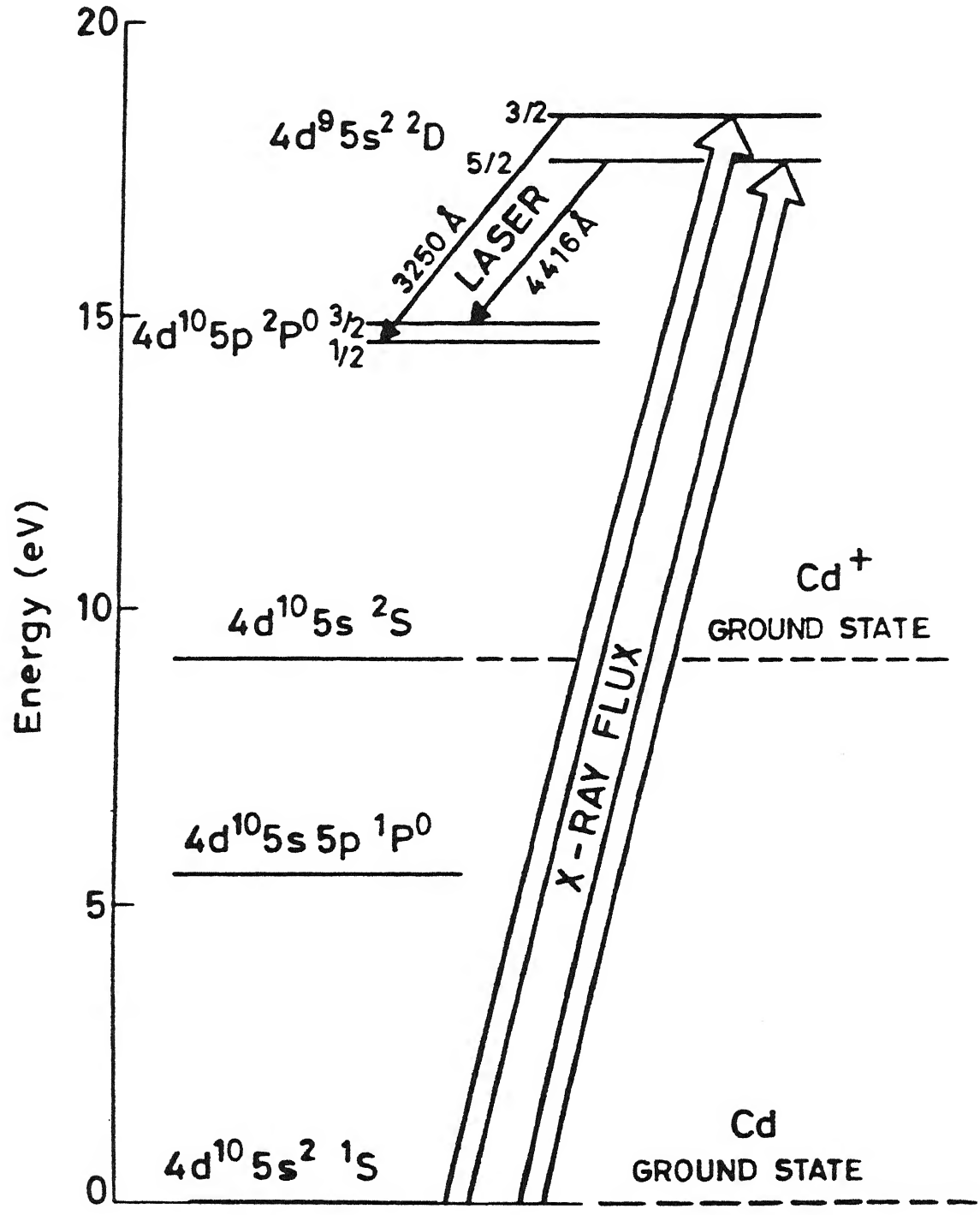

Fig. 24 Energy level diagram for Cd photo-ionization laser.

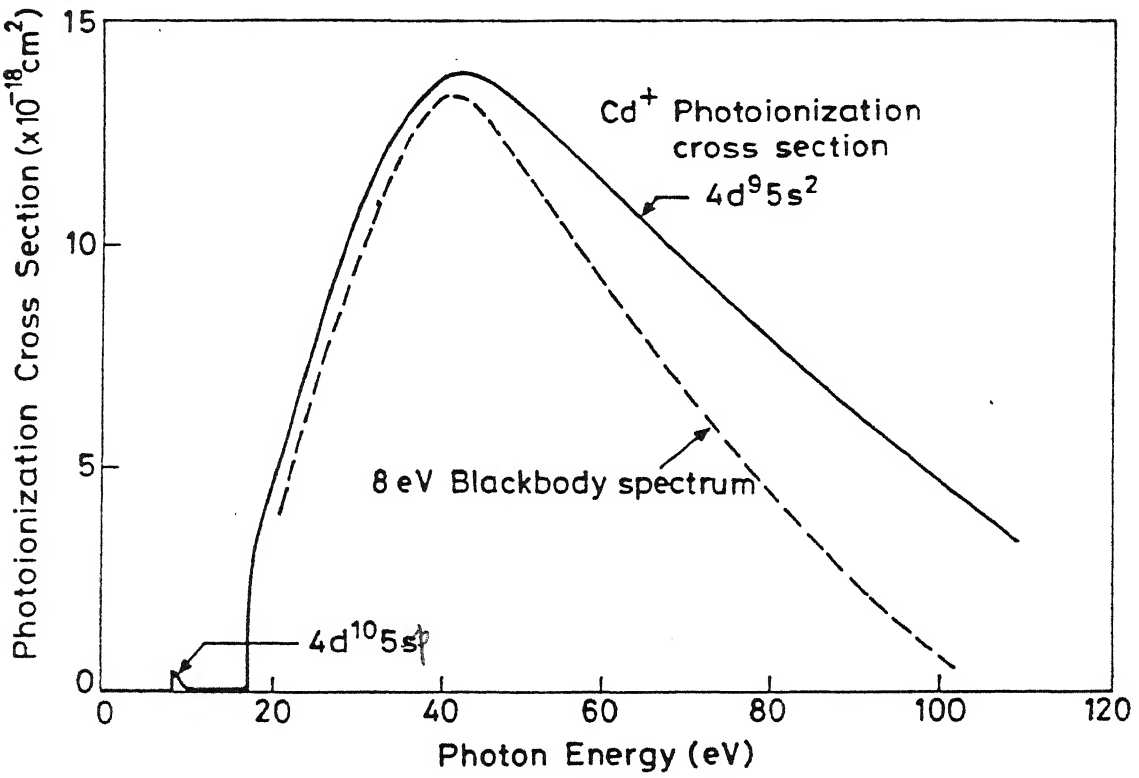

Fig. 25 Photo-ionization cross section of Cd and a spectrum of an 8 eV black body.

EXPERIMENTAL

The experimental set-up used for observing laser oscillations in Cd at 441.6 nm is shown in Fig. 26. A crossed heat pipe of 1 inch dia was used to produce homogeneous vapors of cadmium. The design of the heat pipe used in our studies is described in Chapter II. A tungsten target was inserted from one arm of the heat pipe close to its center. The target was rotated with an electric motor to avoid crater formation. The heat pipe was operated at 420°C and helium at a pressure of 7 Torr was used as a buffer gas. Using a temperature controller it was ensured that temperature of the heat pipe remains within ±5°C. During this temperature variation, the vapor pressure of the cadmium remains nearly constant. We observed[42] the formation of clusters of Cd at the cold zones of the heat pipe if the temperature of the heat pipe was raised above 500°C. A Q-switched Nd:YAG laser delivering upto 1 J of energy in 8 nsec (FWHM) pulse at fundamental was used for plasma production. We used maximum energy of 300 mJ in our studies. The laser radiation was focussed to a 100 μm spot onto the tungsten target using a 18 cm focal length quartz lens. Two He-Cd mirrors of 2 m radius of curvature formed the cavity. One of

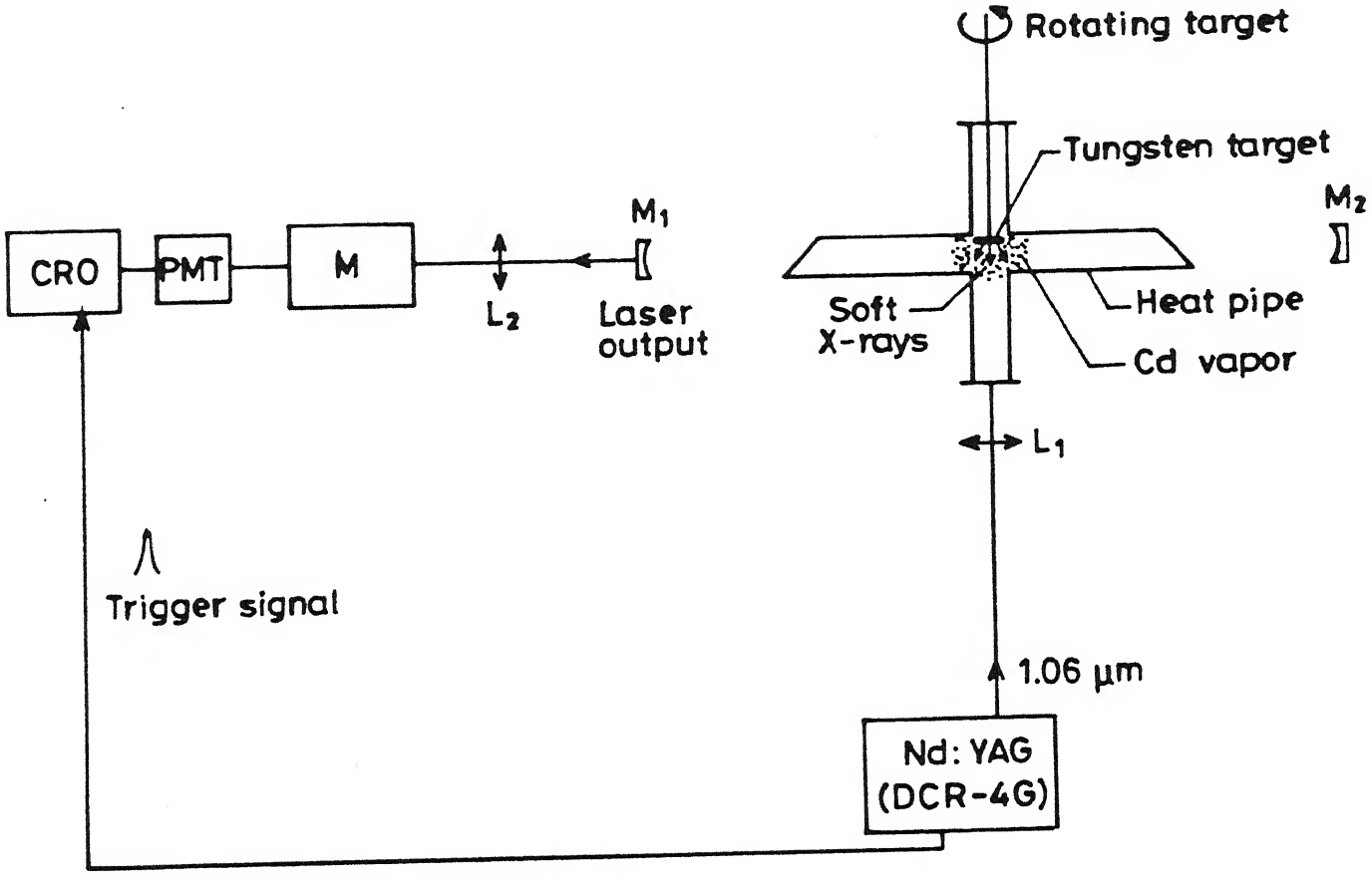

L_1, L_2-Lenses; M-Monochromator; PMT-Photomultiplier Tube; CRO-Storage Oscilloscope; M_1, M_2-Mirrors

Fig. 26 Experimental set up.

the mirror was totally reflecting while the other has about 1 % transmission at 441.6 nm, through which the laser output was monitored. The ends of the heat pipe along the axis of the resonator were fitted with windows set at Brewster angle. The optical axis of the resonator is parallel to the target (tungsten) surface. The output signal is sensitive to the alignment of the resonator axis, with a slight movement of either mirrors the stimulated emission falls to a very low value. The output was detected through a monochromator (HRS-2 Jobin-Yvon) using a photomultiplier tube (IP28, Hamamatsu, rise time 2.2 nsec). The signal was seen on a storage oscilloscope.

To determine the density of cadmium plasma (in the presence of tungsten plasma) a Mach Zehnder Interferometer[37] was designed. Fig. 21 shows the experimental set up for density measurement. The interference fringes at various distances from the target were recorded on a panchromatic film using a lens less camera. The interferograms, thus obtained were analysed using Abel inversion[51] technique. Figs. 27(a) and 27(b) shows the radial profile of electron density at a distance of 4 mm and 5 mm parallel to the target surface.

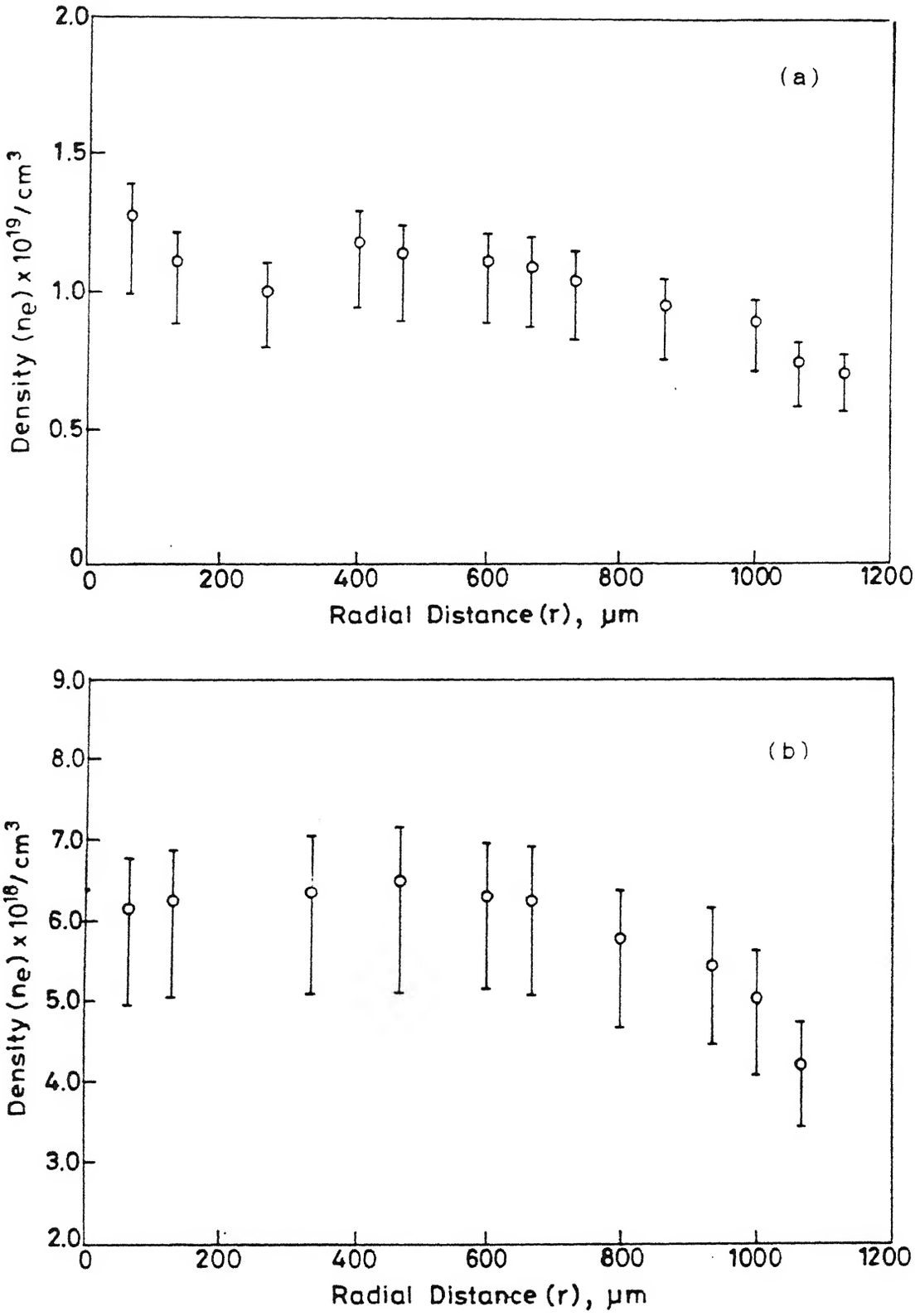

Fig. 27 Radial density profile

(a) at 4 mm from the tungsten target surface

(b) at 5 mm from the tungsten target surface

RESULTS AND DISCUSSIONS

Fig. 28 shows the typical laser pulses recorded using different input energies. To see the effect of the input laser energy (Nd:YAG) on the output of Cd II laser at 441.6 nm, experiment was performed at 100, 200 and 300 mJ of input energy. We observe that the Cd II laser output increases with the input laser energy as shown in Fig. 29. Because of target itching at high input energies we were not able to record the laser pulses but it is expected[98] that the laser output will increase with input energy. Though we observed laser oscillations close to the target surface, the optimum position of the resonator axis is found to be 4 mm away and parallel to the target surface. Since very close to the target surface the pumping flux is high so one expects high inversion densities but electron collisions depopulate the upper laser level. At larger distances the output is decreased due to the reduced pumping flux from the diverging x-rays. The coupling efficiency of the pumping flux and the lasing plasma depends on the configuration used for photoionizing source and metal vapor plasma.

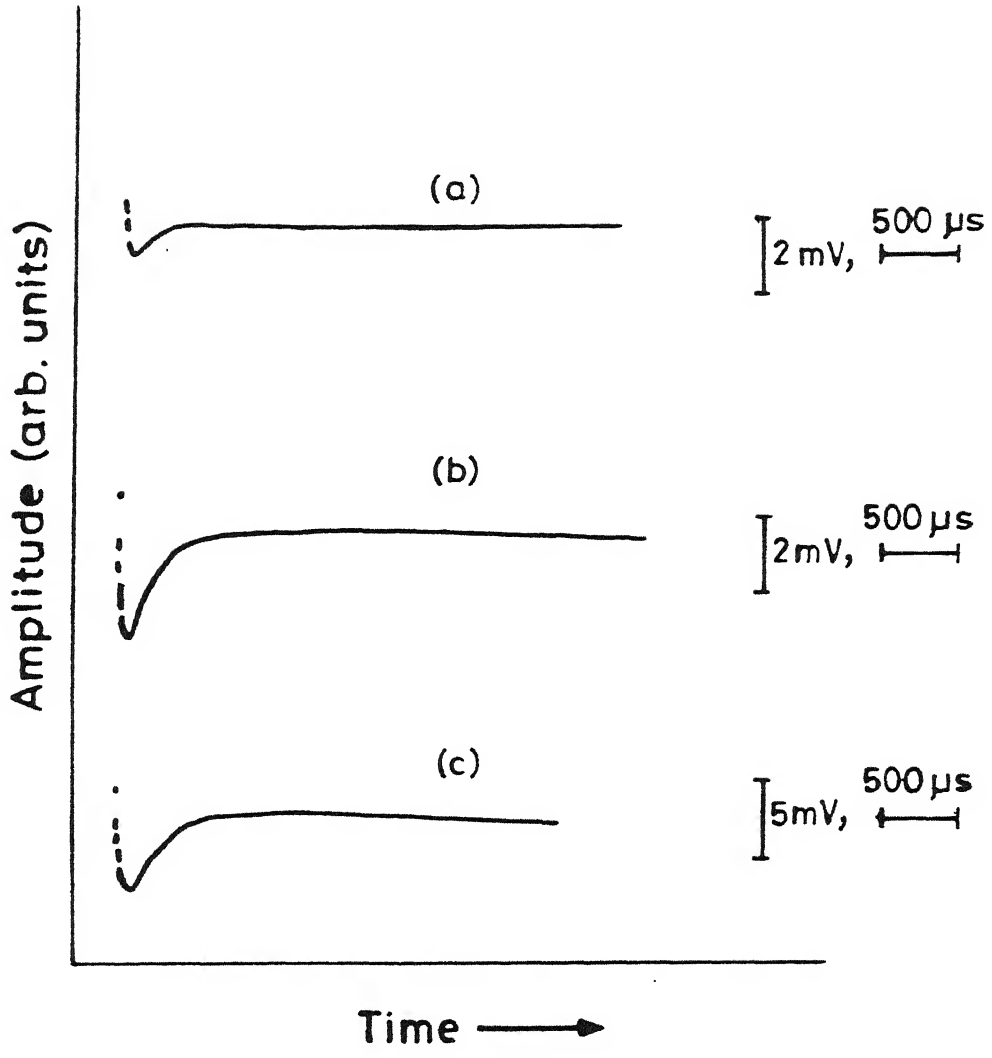

Fig. 28 Oscilloscope traces of laser pulses at various input energies :

(a) E = 100 mJ

(b) E = 200 mJ

(c) E = 300 mJ.

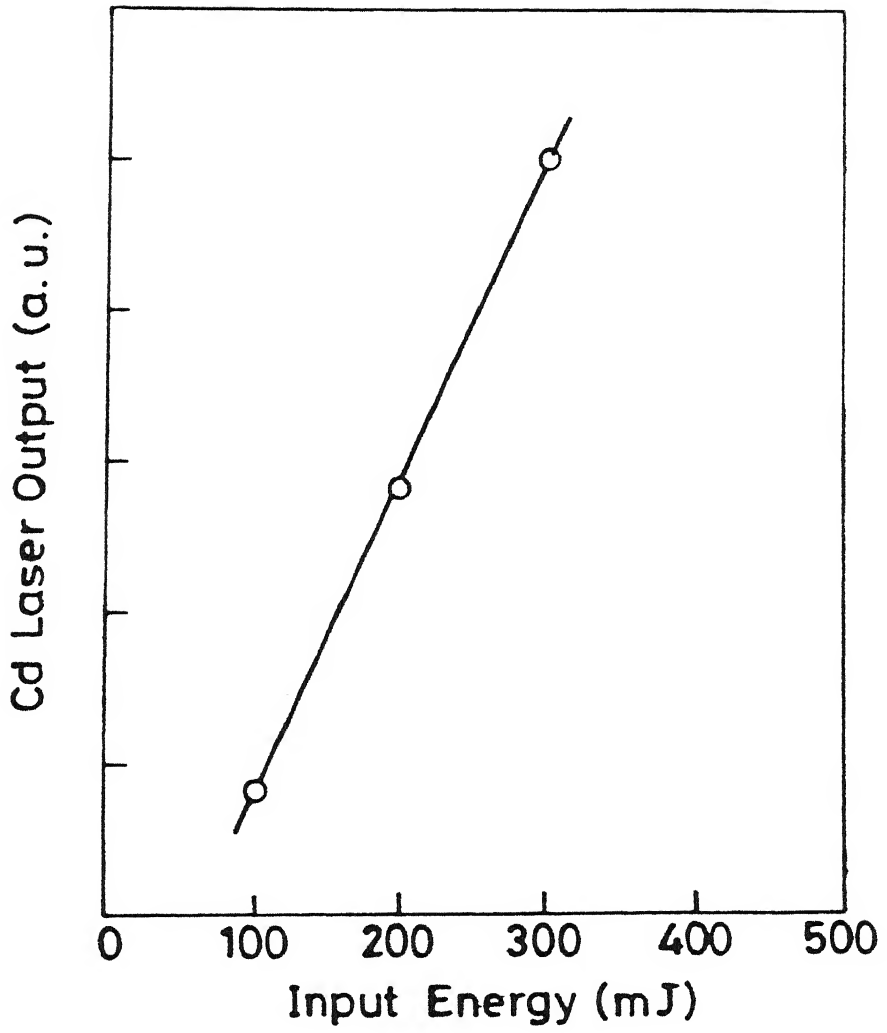

Fig. 29 Variation of Laser output with input energy.

POPULATION INVERSION

Population inversion in photo-ionization lasers can be produced either by directly pumping the upper laser level or transferring population from a nearby directly pumped level to the upper laser level. It has been shown[31] that the latter is less efficient possibly due to broadening of the laser transition during the transfer process. Population inversion[1] from states that are pumped by photo-ionization are also possible to lower lying bound or autoionizing states. The lower laser level being ground state of an ion. For such an inversion to occur the duration of the pumping source should be small so that efficient inversion is produced before electrons collide with neutral species and ionize them to produce ion ground state species. The pump rate coefficient for photo-ionization is given by eq. (1) as

$$P_{pi} = N_{\nu} \sigma_{pi} c \quad sec^{-1} \qquad (1)$$

N_{ν} is the density of photon from a laser produced plasma source interacting with metal vapor and σ_{pi} the photo-ionization cross section to the upper laser level. Photon density N_{ν} from laser

produced plasma at a distance r from the target surface is given by

$$N_{\nu}(r) = N_{\nu} \frac{A}{A(r)} \qquad (18)$$

where A is the area of the pumping source on the target and A(r) is the area at a distance r from the target. From Fig. 30, the solid angle Ω is

$$\Omega = \frac{A(r)}{r^2}$$

if $\Omega = \pi/2$, $A(r) = (\pi/2)r^2$ and eq. (18) becomes

$$N_{\nu}(r) = N_{\nu} \frac{A}{(\pi/2)r^2} \qquad (19)$$

In terms of pumping power the photon density is

$$N_{\nu} = \frac{W_p}{h\nu_p} \frac{1}{c} \frac{1}{A} \qquad (20)$$

where W_p is the power of the pumping source and $h\nu_p$, the energy of the pumping photon. From eq. (19) and (20) we get

$$N_{\nu}(r) = \frac{2W_p}{h\nu_p} \frac{1}{c} \frac{1}{\pi r^2} \qquad (21)$$

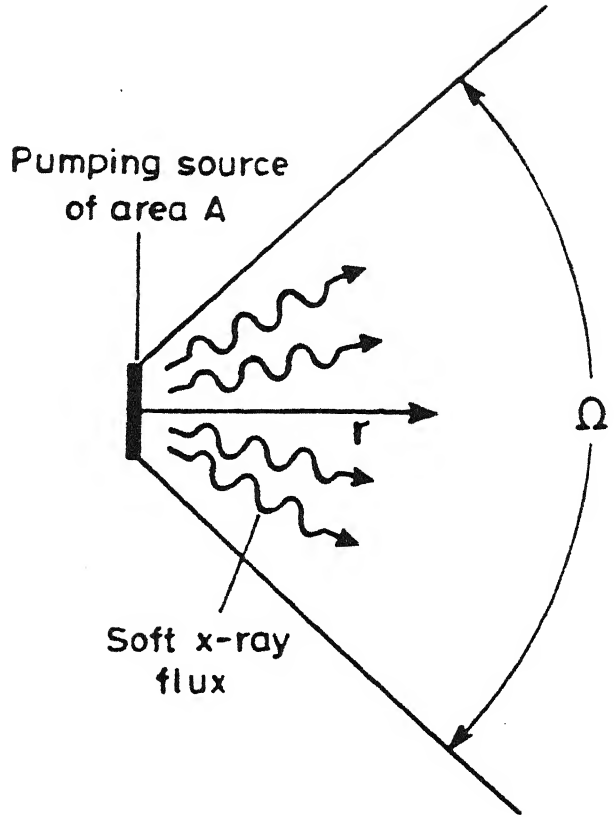

Fig. 30 Pumping geometry showing expansion of plasma in metal vapor.

The emission from the laser produced plasma source is absorbed as it propagates into the vapor medium, and hence the photon density at a distance r becomes

$$N_{\nu}(r) = \frac{2W_p}{h\nu_p} \frac{1}{c} \frac{1}{\pi r^2} e^{-\sigma_t N r} \qquad (22)$$

where N is the ground state population of the metal vapor and σ_t is the total absorption cross section in the wavelength region that pumps the upper laser level. Using eq. (22) in eq. (1) the pump rate coefficient at a distance r from the target surface becomes

$$P_{pi} = \frac{2W_p \sigma_{pi} \exp(-\sigma_t N r)}{h \nu_p \pi r^2} \qquad (23)$$

The population of the upper level is related to the ground state population as

$$N_u = P_{pi} \tau_P N \qquad (24)$$

where τ_P is the duration of the pumping x-ray pulse and is of same duration as that of the laser pulse used for creating soft x-rays. Using eq. (23) in eq. (24) we have,

$$N_u = \frac{2W_p \sigma_{pi} \exp(-\sigma_t Nr)\tau_p N}{h\nu_p \pi r^2} k_f \qquad (25)$$

where k_f is the conversion efficiency of the incident flux into soft x-ray flux. Thus for larger population of the upper state, the photon density N_ν, and the ground state population N should be large. Also the distance between active medium and the pumping source should not be large. $\Delta N = N_u - N_l$ where N_u, N_l are the population densities of upper and lower laser level defines the population inversion. The gain length product GL at a distance of 4 mm from the target, can be calculated from

$$GL \simeq N_u \sigma_{se} L \qquad (26)$$

where N_u is the population density of the upper level and, σ_{se} is the stimulated emission cross section for the lasing wavelength (441.6 nm), L is the length of the gain medium. Substituting the value of N_u from eq. (25), eq. (26) becomes

$$GL = \frac{2W_P \sigma_{pi} \exp(-\sigma_t N r)\, \tau_p N \sigma_{se} L}{h\nu_p \pi r^2} k_f \qquad (27)$$

Using the values of various parameters viz., the stimulated cross section $\sigma_{se} = 7.8\times10^{-18} m^2$ (at 4 mm from the

target) pump power W_p at 300 mJ of the incident 1.06 μm laser radiation 37.5 mW, the partial photo-ionization cross section $\sigma_{pi} = 5\times10^{-22} m^2$ and the total absorption cross section $\sigma_t = 10^{-21} m^2$, cadmium vapor density N at 420°C being $2.78\times10^{-22} m^{-3}$ and the duration of the x-ray pulse is 8.0 nsec (same as 1.06 μm pulse). It follows from eq. (27) that GL~11 (with k_f= 1%). The value of GL apart from other parameters depend on conversion efficiency k_f which depends on configuration, focussing condition, pulse width and wave length of laser used for generation of photo-ionization source.

In conclusion, we have observed laser oscillations in Cd II on $4d^9\ 5s^2\ ^2D_{5/2}$ - $4d^{10}\ 5p\ ^2P_{3/2}$ transition at 441.6 nm using photo-ionization pumping scheme, in a crossed heat pipe. A laser produced tungsten plasma was used as a pumping source. The electron density was estimated using a Mach Zehnder Interferometer and was found to be 1.4×10^{19} cm^{-3} at 4 mm from the target surface.

CHAPTER VI

CONCLUSIONS

We have used photo-ionization pumping scheme to observe laser oscillations in Cd II on $4d^9\ 5s^2\ ^2D_{5/2} - 4d^{10}\ 5p\ ^2P_{3/2}$ transition at 441.6 nm in a crossed heat pipe using tungsten plasma as a pumping source. A Q-switched Nd:YAG laser was used for plasma production. Studies on cadmium metal vapor plasma were also performed in heat pipe. Laser produced aluminium plasma was studied using Nd:YAG laser and its harmonics,to see the dependence of the electron temperature on laser wavelength and intensity. While checking the laser parameters, studies on laser induced air breakdown using Nd:YAG laser, and its harmonics $2\omega_o$, $3\omega_o$, $4\omega_o$ were also performed to see the variation of threshold intensity with pressure and pulse width. We observed the dependence of breakdown threshold intensity on pressure to be between $p^{-0.8}$ and $p^{-0.4}$ and pulse width dependence between $\tau_p^{-0.5}$ and $\tau_p^{-0.35}$.

Cadmium vapor plasma was studied in a crossed heat pipe. Cluster formation was observed in the overheated zones of the heat pipe. A weak He-Ne laser was used to confirm the cluster

formation. The optimum temperature of the heat pipe, free from any cluster formation was 420°C. The temperature of the vapor plasma was estimated to be 0.5 eV by assuming the plasma to be in LTE. Vapor plasma was also studied in the presence of a tungsten (high Z) target. Increase in intensities of all the cadmium lines were observed in the presence of tungsten plasma. The density of plasma was estimated by using a Mach Zehnder Interferometer, in which the heat pipe forms one arm of the Interferometer. Second harmonic (0.532 μm) of the Nd:YAG was used as a probe beam. The analysis of the interferograms were carried out using Abel inversion. The electron density at 2 mm from the tungsten target is estimated to be ~$6 \times 10^{18}/cm^3$.

Studies on laser produced Al plasmas were performed in a vacuum chamber. A Q-switched Nd:YAG laser and its harmonics, were used for plasma production. The electron temperature estimated, by assuming the plasma to be in LTE lies between 0.8 $\leq T_e$ 4.0 eV. The variation of the electron temperature with wavelength for constant intensity shows $\lambda^{-0.3}$ dependence. The temperature varies with laser intensity as $I^{0.3}$, which is close to the $I^{4/9}$ dependence predicted theoretically. The Stark

broadened profile of Al II on 4p $^1P_1$-4d $^1D_2$ transition at 559.3 nm recorded at different distances from the target was used to estimate the electron density profile. The density show $r^{-0.7}$ dependence, where r is the distance from the target. The temporal profile of Al I (396.1 nm), Al II (559.3 nm) and Al III (569.6 nm) lines were used to estimate the velocity of the plasma front.

Laser oscillations in Cd II at 441.6 nm were observed in a crossed heat pipe. Soft x-ray emission from a tungsten plasma was used as a pumping source. Laser resonator was formed with two dielectric coated mirrors with radius of curvature of 2m. The optimum position of resonator axis was found to be 4 mm away and parallel to the tungsten target. To see the effect of input laser energy (Nd:YAG) on the output of Cd II laser at 441.6 nm, experiment was performed at 100, 200, 300 mJ of input energy in 8.0 nsec (FWHM) pulse. An increase in laser output of Cd II was observed with the input energy. The gain length product GL, from our experimentally measured quantities comes out to 11. The density of the cadmium plasma in the presence of tungsten plasma was determined by Mach Zehnder

Interferometer. The density at 4 mm from the target is found to be 1.49×10^{19} cm^{-3}.

Future Aspects

The laser oscillations at 441.6 nm were observed using only one focus spot on the target. However, to increase the length of the gain medium and hence the laser output, we expect multifoci configuration will yield larger output. Since the gain directly depends on the conversion efficiency of 1.06 μm radiation into soft x-rays for high Z, a systematic study for various high Z targets irradiated with short wavelengths should be undertaken to estimate conversion efficiency. Also since the gain depends on geometry of pumping source, studies should be performed with line focus, multiline focus in addition to spherical focus. We have used Nd:YAG laser with pulse width 8.0 nsec (FWHM) for plasma production, electron collisions depopulates the upper laser level and hence the gain is low near the target. The use of short pulses (~100 psec) for plasma production might produce higher gain near the source before collisional deexcitation can occur.

We measured the electron density using a Mach Zehnder Interferometer with 0.532 μm as a probe beam. To estimate the population inversion of the lasing transition at 441.6 nm population density of the upper and lower level should be known. One way to estimate the density of lower level is to use a probe beam, also tuned to 441.6 nm. The resonance absorption at 441.6 nm will show hook structure in the interferograms and the population density can be estimated by measuring the hook separation.

REFERENCES :

1. M.A. Duguay and P.M. Rentzepis, Appl. Phys. Lett. **10**, 350 (1967).

2. S.E. Harris, J.R. Young, R.W. Falcone, J.E. Rothenberg, J.R. Willison, and J.C. Wang, in *Laser Techniques for Extreme Ultraviolet Spectroscopy*, T.J. McIlrath and R.R. Freeman, eds. (American Institute of Physics, New York, 1982), p.147.

3. W.T. Silfvast, J.J. Macklin, and O.R. Wood II, Opt. Lett. **8**, 551 (1983).

4. A.J. Mendelsohn and S.E. Harris, Opt. Lett. **10**, 128 (1985)

5. W.T. Silfvast and O.R. Wood II, J. Opt. Soc. Am. **B4**, 609 (1987).

6. M. Hube, J. Michael, and B. Wellegehausen, Opt. Lett. **15**, 480 (1990).

7. M. Hube, M. Dieckmann, H. Welling, and B. Wellegehausen, J. Opt. Soc. Am. **B6**, 1217 (1989).

8 H. Lundberg, J.J. Macklin, W.T. Silfvast, and O.R. Wood II, Appl. Phys. Lett. **45**, 335 (1984).

9. H.C. Kapteyn and R.W. Falcone, Phys. Rev. **A37**, 2033 (1988).

10. A.M. Weigold and J.A. Piper, Opt. Lett. 15, 1209 (1990).

11. T.N. Lee, E.A. McLean, and R.C. Elton, Phys. Rev. Lett. 59, 1185 (1987).

12. B.J. MacGowan, S. Maxon, P.L. Hagelstein, C.J. Keane, R.A. London, D.L. Mathews, M.D. Rosen, J.H. Scofield, and D.A. Whelan, Phys. Rev. Lett. 59, 2157 (1987).

13. S. Maxon, S. Dalhed, P.L. Hagelstein, R.A. London, B.J. MacGowan, M.D. Rosen, G.Charatis, and G. Busch, Phys. Rev. Lett. 63, 236 (1989).

14. E.L. Latush and M.F. Sem, Sov. Phys. JETP 37, 1017 (1973).

15. F.E. Irons and N.J. Peacock, J. Phys. B: Atom. Molec. Phys. 7, 1109 (1974).

16. D.D. McGregor and M. Mitchner, Phys. Fluids. 17, 2155 (1974).

17. T. Hara, T. Ohgo, M. Hamagaki, and T. Dote, Phys. Lett. 111A, 285 (1985).

18. V.A. Bhagavatula and B. Yaakobi, Opt. Commun. 24, 331 (1978).

19. D. Kim, C.H. Skinner, G. Umesh, and S. Suckewer, Opt. Lett. 14, 665 (1989).

20. W.T. Silfvast and O.R. Wood II, Opt. Lett. 7, 34 (1982).

21. Alika Khare and R.K. Thareja, IEEE J. Quant. Elect. QE24, 2525 (1988).

22. Hiroyuki Daido, Katsunobu Nishihara, Eisuke Miura, and Sadao Nakai, J. Opt. Soc. Am. B7, 266 (1990).

23. Pierre Jaeglé, Gérard Jamelot, Antoine Carillon, Annie Klisnick, Alain Sureau, and Hélène Guennou, J. Opt. Soc. Am. B4, 563 (1987).

24. C.C. Popovics, R. Corbett, C.J. Hooker, M.H. Key, G.P. Kichn, C.L.S. Lewis, G.J. Pert, C. Regan, S.J. Rose, S. Sadaat, R. Smith, T. Tonic,and O. Willi, Phys. Rev. Letts. 59, 2161 (1987).

25. R.H. Dixon and R.C. Elton, Phys. Rev. Lett. 38, 1072 (1977).

26. J.P. Apruzese, J. Davis, and K.G. Whitney, J. Phys. B: Atom. Molec. Phys 11, L643 (1978).

27. V.A. Bhagavatula, Appl. Phys. Lett. 33, 726 (1978).

28. Niansheng Qi, Hayrettin Killic, and Mahadevan Krishnan, Appl. Phys. Lett. 46, 471 (1985).

29. Niansheng Qi and Mahadevan Krishnan, Phys. Rev. Lett. 59, 2051 (1987).

30. Niansheng Qi and Mahadevan Krishnan, Phys. Rev. A39, 4651 (1989).

31. J.P. Apruzese and M. Buie, J. Appl. Phys. 70, 1957 (1991).

32. O'Sullivan, J. Phys. B: At. Molec. Phys. 16, 3291 (1983).

33. T.P. Hughes, *Plasma and Laser Light* (Wiley, New York (1975).

34. J.M. Bridges, C.L. Cromer, and T.J. McIlrath, Appl. Opt. 25, 2208 (1986).

35. M.D. Rosen, D.W. Phillion, V.C. Rupert, W.C. Mead, W.L. Kruer, J.J. Thomson, H.N. Kornblum, V.W. Silvinsky, G.J. Caporaso, M.J. Boyle, and K.G. Tirsell, Phys. Rev. 22, 2020 (1979).

36. T. Mochizuki, K. Hirata, H. Ninomiya, K. Nakamura, K. Maeda, S. Horiguchi, and Y. Fujiwara, Opt. Commun. 72, 302 (1989).

37. W.C. Marlow, Appl. Opt. 6, 1715 (1967).

38. C.D. David Jr, Appl. Phys. Lett. 11, 394 (1967).

39. L. Jahreiss and M.C.E. Huber, Phys. Rev. A28, 3382 (1983).

40. W.K. Lee and C.C. Davis, IEEE J. Quant. Elect. QE 22, 569 (1986).

41. H. Ninomiya, N. Takashima, and K. Hirata, J. Appl. Phys. 69, 67 (1991).

42. Rekha Tambay and R.K. Thareja, J. Appl. Phys. (Submitted).

43. T.J. Englert and M.A. Beik, Rev. Sci. Instrum. **61**, 3783 (1990).

44. I.H. Hutchinson, *Principles of Plasma Diagnostics*, (Cambridge University Press, 1987).

45. W.L. Wiese and P.W. Murphy, Phys. Rev. **131**, 2108 (1963).

46. F.E. Irons, J. Phys. B: Atom. Molec. Phys. **6**, 1562 (1973).

47. J. Ashkenazy, R. Kipper, and M. Caner, Phys. Rev. **A43**, 5568 (1991).

48. H.R. Griem, *Plasma Spectroscopy* (McGraw Hill, New York, 1964).

49. A. Khare, V. Kumar, and R.K. Thareja, Z. Phys. D, Atoms. Molecules and Clusters **6**, 67 (1987).

50. Rekha Tambay, Ranjit Singh , and R.K. Thareja, J. Appl. Phys. (Submitted).

51. K. Bockasten, J. Opt. Soc. Am. **51**, 943 (1961).

52. R. Illingworth and R.K. Thareja, J. Phys. E: Sci. Instrum. **14**, 147 (1981).

53. W.R.S. Garton and K. Codling, Proc. Phys. Soc. (London) **75**, 87 (1960).

54. F.S. Tomkins and B. Ercoli, Appl. Opt. **6**, 1299 (1967).

55. G.M. Grover, T.P. Cotter, and G.F. Erickson. J. Appl. Phys. 35, 1990 (1964).

56. C.R. Vidal, J. Appl. Phys. 44, 2232 (1973).

57. H. Scheingraber and C.R. Vidal, Rev. Sci. Instrum. 52, 1010 (1981).

58. W. Gawlik and R. Neumann, Opt. Commun. 68, 345 (1988).

59. Vinay Kumar, Ph.D. Thesis, IIT Kanpur (1989).

60. Rekha Tambay and R. K. Thareja, J. Appl. Phys. 70, 2890 (1991).

61. W.E. Williams, M.J. Soileau, and E.W. Van Stryland, Appl. Phys. Letts. 43, 352 (1983).

62. E.W. Van Stryland, M. J. Soileau, A. L. Smirl, and W. E. Williams, Phys. Rev. B23, 2144 (1981).

63. Rekha Tambay, D. Victor Suvisesha Muthu, V. Kumar, and R.K. Thareja, Pramana J. Phys. 37, 163 (1991).

64. E.T. Kennedy, Contemp. Phys. 25, 31 (1984).

65. N.G. Basov, V.A. Boiko, Yu.P. Voinov, E.Ya. Kononov, S.L. Mandelshtan, and G.V. Sklizkov, JETP Lett. 6, 291 (1967).

66. W.T. Silfvast, L.H. Szeto, and O.R. Wood II, Opt. Lett. 4, 271 (1979).

67. V.I. Bayanov, V.A. Serebryakov, I. Yu. Skobelev, N.A. Solóvev, A. Ya. Faenov, and S. Ya. Khakhalin, Sov. J. Quant. Elect. 18, 1150 (1988).

68. A.P. Golúb and I.V. Nemchinov, J. Europ. Phys. 59, 852 (1990).

69. H. Nishimura, F. Matsuoka, M. Yagi, K. Yamada, S. Nakai, G.H. McCall, and C. Yamanaka, Phys. Fluids. 26, 1688 (1983).

70. J. Bruneau, A. Decoster, D. Desenne, H. Dumont, J. P Le Breton, M. Boivineau, J. P. Perrine, S. Bayle, M. Louis-Jacquet, J.P. Geindre, C. Chenais-Popovics, and J.C. Gauthier, Phys. Rev. A44, R832 (1991).

71. J.A. Mckay, R.D. Bleach, D.J. Nagel, J.T. Schriempf, R.B. Hall, C.R. Pond, and S.K. Manlief, J. Appl. Phys. 50, 3231 (1979).

72. C. Timmer, S.K. Srivastava, T.E. Hall, and A.F. Fucaloro, J. Appl. Phys. 70, 1888 (1991).

73. P.A. Naik, P.D. Gupta, and S.R. Kumbhare Phy Rev 43, 4540 (1991).

74. V. Kumar and R.K. Thareja, J. Appl. Phys. 67, 3260 (1990).

75. J.A. Cobble, G.T. Schappert, L.A. Jones, A.J. Taylor, G.A. Kyrala, and R.D. Fulton, J. Appl. Phys. 69, 3369 (1991).

76. J. Abdallah Jr and Robert E.H. Clark J. Appl. Phys. 69, 23 (1991).

77. J.E. Rothenberg and G. Koren, Appl. Phys. Lett. 44, 664 (1984).

78. J.T. Knudston, W.B. Green, and D.G. Sutton, J. Appl. Phys. 61, 4771 (1987).

79. A.R. Striganov and N.S. Sventitskii, in *Tables of Spectral Lines of Neutral and Ionized Atoms* (Plenum: New-York - Washington 1968).

80. H. Puell, Z. Naturforsch 25A, 1807 (1970).

81. G.J. Pert, *Laser Plasma Interaction Proceedings of the Twentieth Scottish Universities Summer School in Physics 1979* (ed. by R.A. Cairns and J.J. Sanderson).

82. G. Bekefi, *Principles of Laser Plasmas* (Wiley, New York, (1976).

83. C.R. Vidal and J. Cooper, J Appl. Phys. 40, 3370 (1969)

84. C.R. Vidal, Appl. Opt. 19, 3897 (1980).

85. K. Miyazaki, H. Sakai, and T. Sato, Opt. lett. 9, 457 (1984).

86. D.C. Hanna, M.A. Yuratich, and D. Cotter, *Nonlinear optics of Free Atoms and Molecules*, Springer Series in Optical Sciences, Vol 17. (Springer, Berlin, 1979).

87. R.G. Caro, J.C. Wang, J.F. Young, and S.E. Harris, Phys. Rev. A30, 1407 (1984).

88. A. Tünnermann, H. Eichmann, R. Henking, K. Mossavi, and B. Wellegehausen, Opt. Lett. 16, 402 (1991).

89. M.M. Hessel and T.B. Lucatorto, Rev. Sci. Instrum. 44, 561 (1973).

90. A. Sharma, Opt. Commun. 77, 303 (1990).

91. M. Allegrini, P. Bicchi, D. Dattrino, and L. Moi, Opt. Commun. 49, 39 (1984).

92. R. Ramis and J.R. Sanmartin, Nucl. Fusion. 23, 739 (1983).

93. E.J. McGuire, Phys. Rev. Lett. 35, 844 (1975).

94. S.A. Mani, H.A. Hyman, and J.D. Daugherty, J. Appl. Phys. 47, 3099 (1976).

95. S.E. Harris, R.W. Falcone, M. Gross, R. Normandin, K.D. Pedrotti, J.E. Rothenberg, J.C. Wang, J.R. Willison, and J.R. Young, in *Laser Spectroscopy V*, A.R.W. McKeller, T. Oka, and B.P. Stoicheff, Eds. (Springer-Verlag, New York, 1981), pp. 437.

96. H.A. Hyman and S.A. Mani, Opt. Commun. 20, 209 (1977).

97. R.G. Caro, J.C. Wang, J.F. Young, and S.E. Harris, Phys. Rev. A30, 1407 (1984).

98. M. Hube, R. Brinkman, H. Welling, R. Beigang, and B. Wellegehausen, Appl. Phys. B45, 197 (1988).